



THE UNIVERSITY OF
SYDNEY

THE UNIVERSITY OF SYDNEY

HONOURS THESIS

**Reverse Engineering Natural Flight:
Wind Tunnel Investigation of
Membranous Wings**

Name:

REAGAN YA PENG LUO

Student ID:

500 586 679

Supervisor: DR. ZIHAO WANG

*A thesis submitted in fulfilment of the requirements for the degree of
Bachelor of Aeronautical Engineering (Space) Honours in the*

School of Aerospace, Mechanical, and Mechatronic Engineering
Faculty of Engineering

AMME4112 - THESIS B

OCTOBER 31, 2024

This page is intentionally left blank.

Abstract

[REMINDER: Write the actual abstract here. This abstract should provide a concise summary of the entire report, covering the following points:

- **Objective:** Briefly describe the purpose of the study or project. Why is it important?
- **Methodology:** Summarize the methods used. Include any specific techniques, tools, or experiments conducted to achieve your objectives.
- **Key Results:** Highlight the most significant findings or outcomes. What are the primary insights gained?
- **Conclusion:** Conclude with the implications of your results. How do they contribute to the field, and what future work might be suggested?

Aim for a word count of 150-250 words to keep the abstract concise but informative.]

This page is intentionally left blank.

Statement of Contribution

- i fucked you mother last night while your daddy ran away
- i fucked you mother last night while your daddy ran away
- i fucked you mother last night while your daddy ran away
- i fucked you mother last night while your daddy ran away
- i fucked you mother last night while your daddy ran away
- i fucked you mother last night while your daddy ran away
- i fucked you mother last night while your daddy ran away

The above is an accurate representation of the work the student has completed:

STUDENT: REAGAN YA PENG LUO

DATE

SUPERVISOR: DR. ZIHAO WANG

DATE

This page is intentionally left blank.

Acknowledgements

First and foremost, I would like to express my deepest gratitude to my supervisor, Dr. [Supervisor's Name], for their invaluable guidance, support, and encouragement throughout the course of my research and thesis writing. Their insights, patience, and constant feedback were instrumental in shaping this work and helping me navigate the many challenges encountered along the way. I am immensely grateful for their mentorship and the numerous hours they spent refining my ideas and approaches.

Lorem ipsum dolor sit amet, consectetur adipiscing elit. Ut purus elit, vestibulum ut, placerat ac, adipiscing vitae, felis. Curabitur dictum gravida mauris. Nam arcu libero, nonummy eget, consectetur id, vulputate a, magna. Donec vehicula augue eu neque. Pellentesque habitant morbi tristique senectus et netus et malesuada fames ac turpis egestas. Mauris ut leo. Cras viverra metus rhoncus sem. Nulla et lectus vestibulum urna fringilla ultrices. Phasellus eu tellus sit amet tortor gravida placerat. Integer sapien est, iaculis in, pretium quis, viverra ac, nunc. Praesent eget sem vel leo ultrices bibendum. Aenean faucibus. Morbi dolor nulla, malesuada eu, pulvinar at, mollis ac, nulla. Curabitur auctor semper nulla. Donec varius orci eget risus. Duis nibh mi, congue eu, accumsan eleifend, sagittis quis, diam. Duis eget orci sit amet orci dignissim rutrum.

Nam dui ligula, fringilla a, euismod sodales, sollicitudin vel, wisi. Morbi auctor lorem non justo. Nam lacus libero, pretium at, lobortis vitae, ultricies et, tellus. Donec aliquet, tortor sed accumsan bibendum, erat ligula aliquet magna, vitae ornare odio metus a mi. Morbi ac orci et nisl hendrerit mollis. Suspendisse ut massa. Cras nec ante. Pellentesque a nulla. Cum sociis natoque penatibus et magnis dis parturient montes,

nascetur ridiculus mus. Aliquam tincidunt urna. Nulla ullamcorper vestibulum turpis. Pellentesque cursus luctus mauris.

Nulla malesuada porttitor diam. Donec felis erat, congue non, volutpat at, tincidunt tristique, libero. Vivamus viverra fermentum felis. Donec nonummy pellentesque ante. Phasellus adipiscing semper elit. Proin fermentum massa ac quam. Sed diam turpis, molestie vitae, placerat a, molestie nec, leo. Maecenas lacinia. Nam ipsum ligula, eleifend at, accumsan nec, suscipit a, ipsum. Morbi blandit ligula feugiat magna. Nunc eleifend consequat lorem. Sed lacinia nulla vitae enim. Pellentesque tincidunt purus vel magna. Integer non enim. Praesent euismod nunc eu purus. Donec bibendum quam in tellus. Nullam cursus pulvinar lectus. Donec et mi. Nam vulputate metus eu enim. Vestibulum pellentesque felis eu massa.

Thank you all for being a part of this journey. Your support has been invaluable, and I dedicate this work to you.

REAGAN YA PENG LUO

Contents

Abstract	i
Statement of Contribution	iii
Acknowledgements	v
1 Introduction	1
1.1 Motivation	1
1.2 Research Objectives	3
1.2.1 High-Level Goals	3
1.2.2 Low-Level Goals	3
1.3 Thesis Outline	3
2 Literature Review	5
2.1 Aerodynamic Fundamentals in Natural and Engineered Flight	5
2.1.1 Principles of Aerodynamics	5
2.1.2 Wing Morphology Across Species	6
2.1.3 Aerodynamic Effects of Wing Morphology	9
2.1.4 Surface Textures and Their Aerodynamic Implications	9
2.1.5 Empirical Data from Wind Tunnel Tests	9
2.2 Mathematical Background	12
2.2.1 Lift and Drag Coefficients	12
2.2.2 Dimensionless Properties: Reynolds Number	12
2.3 Wind Tunnel	13

2.3.1	Background of Wind Tunnel Testing	13
2.3.2	Boundary Layer and Effects	14
2.3.3	Classical Correction Factors	15
2.4	Case Studies of Existing Ornithopters	16
2.4.1	RoboFalcon	16
2.4.2	Korean Bioinspired Ornithopter	18
2.4.3	Scibilia and Wojciechowski Model	20
2.4.4	MEMS Wing Ornithopter	22
2.4.5	Srigrarom and Chan Model	23
2.4.6	FESTO - SmartBird	25
2.4.7	Summary of all Case Studies and Contributions	28
2.4.8	Proposed Solution	29
3	Methodology	31
3.1	Wing Kinematic Design	31
3.1.1	Bio-inspiration	32
3.1.2	Computerised Design	33
3.2	Material Properties and Choices	34
3.2.1	Material Selection Overview	34
3.2.2	Material Descriptions	35
3.3	Manufacturing and Assembly	36
3.3.1	Fabrication Techniques and Justifications	36
3.3.2	Assembly	43
4	Wind Tunnel Methodology	45
4.1	Wind Tunnel Preparation and Setup	45
4.1.1	Wind Tunnel Specifications	45
4.1.2	Test Section Setup	45
4.2	Testing and Post Processing	48
4.2.1	Test Types	48
4.2.2	Post Processing	49

5 Results and Discussion	51
5.1 Baseline Results	51
5.2 Pseudo-Static Results	51
5.3 Dynamic Results	51
5.4 Comparison with Analytical Results	51
6 Conclusions	53
6.1 Final Thoughts	53
6.2 Further Improvements	53
6.3 Contributions and Achievements	53
Bibliography	i
Appendices	viii
A Progress to Date	ix
A.1 Investigation into Tucking Kinematics	ix
A.2 Progress Tracking	xi
A.3 Proceeding Semester work	xii

This page is intentionally left blank.

List of Figures

1.1	Leonardo da Vinci Flying Machine [1]	2
2.1	Vortex Generation by a Falcon	6
2.2	Comparison of flight mechanics between the albatross and sparrow	8
2.3	Spreading of Feathers to Increase Wingspan [10]	8
2.4	Nighthawk Wing. LEFT: lift coefficient (C_L) as a function of drag coefficient (C_D). RIGHT: lift coefficient (C_L), drag coefficient (C_D), and lift/drag ratio (C_L/C_D) at differing angles of attack (α) [14]	11
2.5	Aeromech Wind Tunnel 8m \times 10m [22]	13
2.6	Boundary Layer Wall Depiction [26]	14
2.7	RoboFalcon Ornithopter in Flight [30]	16
2.8	RoboFalon Wing Mechanism [30]	17
2.9	Korean Bioinspired Ornithopter with Visual Trackers [31]	19
2.10	Global Wing, Tail, and Body Trajectories of Marker Sets [31]	20
2.11	Moving Wing Mechanism and AOA Control (Scibilia et al. 2006 [32]) .	21
2.12	Fabrication Process of Titanium Alloy MEMS Wings [33]	23
2.13	Srigrarom and Chan First Prototype Ornithopter [34]	24
2.14	Srigrarom and Chan Model Wing Skeletal Structure [34]	25
2.15	Average Lift Force vs Flapping Angle [34]	26
2.16	Front View (A) and X-Ray View (B) of FESTO SmartBird [35]	26
2.17	Top View of FESTO Wing and Torsion Motor Sensor [35]	27
3.1	Wing semi-span planform view, LEFT: small passerine bird, RIGHT: Pall's long-tongued bat [36]	32

3.2 Ornithopter Design Architecture	32
3.3 Photograph of the underside of a bat wing [40]	33
3.4 Wing skeleton in CAD, Choudhury [41]	34
3.5 Labelled Wing Skeleton Materials	37
3.6 Close up of wrist joint design	38
3.7 Hang Gliders, Royal National Park	39
3.8 Fabric and Skeleton Integration	40
3.9 Full Membrane Integration	41
3.10 Gearbox Inner Mechanism	41
3.11 Spur Gear Brass Bearing Shaft	42
3.12 Wind Tunnel Mount Design	42
3.13 Rendered Assemblies	43
3.14 Full Gearbox Assembly	44
3.15 Complete Wing Setup in Wind Tunnel	44
4.1 USYD Low Speed 4×3 feet Wind Tunnel Specifications	46
4.2 Test Section Setups Rendered in SOLIDWORKS	46
4.3 CAD Representation of Phase Angles	49
A.1 CAD Prototype Ornithopter Mechanism	ix
A.2 3D printed wing mechanism	x
A.3 Proposed Gantt Chart	xi

List of Tables

2.1	Morphometric parameters for various bird wings [14]	10
2.2	Lift and pressure drag coefficients calculated for the nighthawk wing [14]	11
2.3	Comparative Analysis of Ornithopter Models	28
3.1	Summary of Material Trade-Offs	36
4.1	Benchmarking Tests for Gearbox Drag, Dry Run, and Membraneless Run	48

Chapter 1

Introduction

“A bird is an instrument working according to mathematical law, which instrument it is within the capacity of man to reproduce with all its movements.”

— Leonardo da Vinci, *Codex Atlanticus*

1.1 Motivation

Unmanned Aerial Vehicles (UAVs), more often known as drones, represent a significantly advancing field. It has deep roots within both the natural world and the ingenuity of the human mind. Initially developed for military applications, UAVs have surpassed their origins and have served in a vast array of civilian and scientific roles. This technological evolution closely resembles that in nature, especially of volant (flying) creatures. Their flight mechanisms have inspired a wide array of aerial technologies, especially more recently with ornithopters.

Ornithopters, from the Greek words for “bird” and “wing,” are aircraft that can propel themselves by flapping their wings, resembling that of birds, bats, and insects. Bio-inspiration has opened many new avenues with unique advantages, such as manoeuvrability and efficiency, coming out on top where conventional drones fall short. The design and studying of ornithopters can help give extremely valuable insights into the mechanics of natural flight, giving us breakthroughs in harnessing biomimicry. As

mentioned by Leonardo da Vinci in his Codex Atlanticus, nature should be used as an instrument where man should reproduce all its movements. He himself devised one of the very first biomimetic designs, inspiring future generations to carry on.

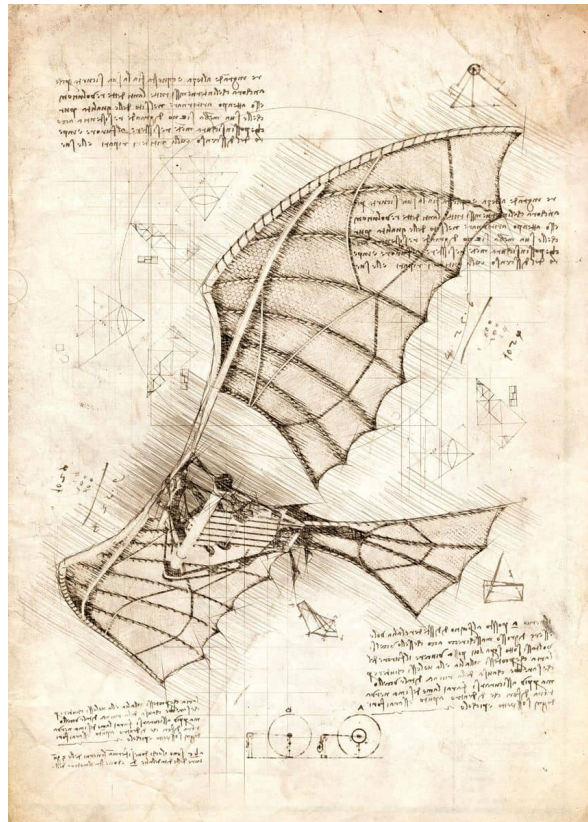


Figure 1.1: Leonardo da Vinci Flying Machine [1]

The potential use of ornithopters in warfare can represent an evolution in military weapons and technology. The natural flight mechanisms of birds and bats, inspired by biomimetic design, allow for extreme stealth, making them ideal for missions requiring penetration into enemy territories. Furthermore, the ability to mimic natural creatures reduces their recognition as threats, allowing them to get close to targets before deployment of any selected payloads.

Electronic and radar detection systems are commonplace in modern warfare, so exploiting biomimicry opens up tactics in aerial offence, surveillance, and reconnaissance. Strategic integration of bio-inspired designs for military UAVs will be revolutionary for the next generation of complex war zone environments.

1.2 Research Objectives

1.2.1 High-Level Goals

- **Contribute to the body of knowledge on bio-inspired flight**, particularly in understanding the mechanics behind the flight of birds and bats
- **Evaluate the feasibility** of incorporating bird and bat wing design principles into the next generation of ornithopters
- **Explore the potential environmental and operational advantages** of ornithopters over conventional drones and aircraft

1.2.2 Low-Level Goals

- **Fabricate bird and bat wing models** based on anatomical studies and aerodynamic principles
- **Conduct wind tunnel tests** to analyse the aerodynamic performance of these wing models under various flight conditions
- **Identify the configurations that yield optimal lift and drag values**, contributing to the efficient design of ornithopter wings

1.3 Thesis Outline

Chapter 1 outlines an introduction, the motivation behind ornithopters, and the use case of these. A small amount of background has been provided on the history of birds.

Chapter 2 provides a detailed literature review of history, basic principles, and existing ornithopter designs and summarises the use of materials and testing objectives.

Chapter 3 describes the construction and approach this paper will use to develop and manufacture this ornithopter.

Chapter 4 shows the wind tunnel setup and usage method. It also includes post-processing of all measured data.

Chapter 5 offers an in-depth discussion of all measured results using the fabricated ornithopter design.

Chapter 6 summarises the contributions of this thesis and suggests limitations and room for further improvement.

Chapter 2

Literature Review

2.1 Aerodynamic Fundamentals in Natural and Engineered Flight

2.1.1 Principles of Aerodynamics

Aerodynamics is a field of study concerning the motion of air. The way it interacts with solid objects is extremely fundamental to understanding flight. All flying objects are influenced by the primary forces of lift and drag due to some method of actuation, including wings. This introduces the concept of lift, perpendicular to the direction of air, which is essential for maintaining flight. On the other hand, drag is also generated as a result of lift and thrust, a quantity which resists forward movement by acting opposite to the direction of motion.

More specifically, lift is generated by Bernoulli's principle. A specifically engineered wing shape causes a difference in air velocity between the top and bottom surfaces, which in turn generates a relatively higher pressure profile on the bottom side. A difference in pressure is the direct effect of this shape and the pressure gradient creates an upwards lift force [2]. Furthermore, Newton's third law of action and reaction forces helps reinforce this explanation. In this specific case, the downwards deflection of air creates the upwards reaction and hence displacement of the wing. The 'spillage' of high

pressure air from the bottom towards the topside results in the creation of vortices, which are seen in both aircraft and avian creatures, picture in **Figure 2.1**.



Figure 2.1: Vortex Generation by a Falcon

Turbulence is another fundamental within aerodynamics. It concerns unpredictable air movement, and happens when smooth (laminar) flow forms into swirls (eddies). Sudden changes in velocity and pressure, due to Bernoulli's principle, causes the effects of turbulence which can significantly impact the aerodynamic performance of a flying object. With aircraft flight, turbulence is highly unfavourable due to its unpredictability and suddenness. This can potentially lead to sharp changes in lift and especially an increase drag, resulting in greatly reduced flight efficiency and increased fuel consumption. Moreover, the flight stability and control is also greatly affected due to the uncertainty with turbulence. On top of this, frequent exposure to turbulence causes an increased amount of cyclical stress on aircraft wings and components. A large amount of engineering must go into accounting for a margin of safety to prevent any potential failure.

On the other hand, many birds and insects show behaviours and have physical adaptations that allow them to deal with and even exploit the use of turbulence. Birds often use this to their advantage by gaining altitude by riding updraughts to gain altitude while expending minimal energy. Eagles, which are soaring birds, are particularly known for gaining altitude by using thermal columns to ascend [3].

2.1.2 Wing Morphology Across Species

Morphology, at a glance in the context of wings, is a study into the structure and shape of wings across a variety of species, mainly concerning birds and insects. This

includes an in-depth examination into the natural architecture of wings, including but not limited to:

- arrangement of feathers
- size and shape of wing bones
- wing veins or membranes [4]

Researchers often have a focus on understanding adaptations for flight, especially how wing morphology affects the aerodynamics, manoeuvrability, and efficiency in different ecological contexts. As an example, birds of prey may have distinct morphological features optimised for soaring and gliding, while hummingbirds' wings are adapted for hovering and rapid manoeuvring.

Through the analysis of wing morphology, scientists gain insights into the evolutionary history, ecological roles, as well as functional capabilities of different wing designs across diverse species [5]. Additionally, studies like Pennycuick's manual on bird flight performance provide valuable insights into the relationship between wing structure and flight capabilities in birds as well as a showcase of sections in wing morphology and especially aerodynamics.

Some examples of bird wing morphology include the wing shape and function. Albatrosses, for example, have long, narrow wings that allow them to glide for long distances over the ocean through the use of wind currents and turbulence [6]. Contrasting to this, forest birds such as sparrows have shorter, rounder wings that enable quick, agile manoeuvres in turbulent air close to tree canopies. A comparison is visualised within **Figure 2.2**.

Feather adaptations also play a critical role in managing aerodynamic forces. The ability to change the positioning of feathers allows birds to both increase and decrease the relative surface area and stiffness. **Figure 2.3** shows a parrot expanding its wing's surface area. It also allows a change in camber, effectively changing lift generation, which is very effective for a response to sudden changes in air currents [9].

Another feature within bird morphology is the *alula*, also displayed in the middle of



(a) Albatross in flight - large wingspan [7]



(b) Sparrow taking off - small wings [8]

Figure 2.2: Comparison of flight mechanics between the albatross and sparrow**Figure 2.3:** Spreading of Feathers to Increase Wingspan [10]

the parrot wing in **Figure 2.3**, which is a small set of feathers on the leading edge of primary wings. It acts as a tiny wing which prevents stalling at high angles of attack, especially in turbulent air [11]. This allows for much better control at slow speeds, most importantly through turbulent conditions.

Bat wings, on the other hand, are quite distinct from those of birds. They feature a flexible skin membrane stretched between elongated fingers. This unique structure also allows for total control over wing shape and stiffness, allowing bats to fly in a variety of different environments.

With reference to bat morphology, wing flexibility is a crucial component. The elasticity within the membrane enables adjustments to loading and surface area. Furthermore, the flexibility allows for energy-efficient flight by minimising drag during upstroke and maximising lift during downstroke [12]. Due to the ability to change wing shape,

counteracting against turbulence is easily done. The morphing capability is also important for their echolocation. This helps precise manoeuvring around obstacles and prey especially in darkness.

2.1.3 Aerodynamic Effects of Wing Morphology

The shape and size of wings play a critical role in flight capabilities. Aspect ratio, the wing span to mean chord ratio, affects generation of lift and energy efficiency. High aspect ratio wings, which are typical of many long-distance flyers, reduce drag and enhance lift efficiency [5]. Low aspect ratio wings are much better for slow speeds or in cluttered environments as mentioned by Spedding in his Mechanics of Animal Locomotion publication [13]. Furthermore, the angle of attack, defined as the angle between wing chord and air flow, is important for the generation of lift as too high a magnitude causes stall. Stall is the separation of airflow of the wing surface, meaning no lift production.

2.1.4 Surface Textures and Their Aerodynamic Implications

Surface texture is another factor which immediately affects aerodynamic performance. As mentioned before, bird feathers can be adjusted, bat wings can be stretched, changing the surface area and angle of attack mid flight. This allows for drag reduction especially in high speed manoeuvres. Within the realm of UAV design, biomimicry can be used to enhance performance, such as the use of adjustable surface or materials that mimic the morphology of feathers and membranes.

2.1.5 Empirical Data from Wind Tunnel Tests

In a paper by P.C. Withers, he provides an extremely extensive aerodynamic analysis of bird wings, focusing on properties when considered as fixed aerofoils. Key findings in this study talk about how wing morphology and aerodynamic performance at a range of Reynolds numbers (Re) affects lift and drag coefficients. More specifically, it was found that bird wings operate at lower Re values compared to typical aircraft aerofoils. This results in higher minimum drag coefficients and lower maximum lift coefficients,

with the difference due to the smaller size and lower flight speeds of birds in general.

Withers' analysis involves studying the aerodynamic performance through empirical data obtained from wind tunnel tests of fixed bird aerofoils. Dried wings in the appropriate gliding position were either taken from frozen birds or borrowed from an ornithology collection. Epoxy resin was used as bonding glue to attach a brass rod within the humerus, connected directly to a force transducer.

Furthermore, Withers discusses the role of wing-tip modifications, which are crucial for managing airflow and improving lift, especially at higher angles of attack. Such modifications can alter the aerodynamic properties significantly, suggesting potential areas for further research and application in bio-inspired aerofoil design.

Table 2.1 displays a variety of different bird wings analysed as fixed aerofoils, where the thickness ratio = maximum thickness/chord, camber ratio = maximum deviation of centre of wing from line connecting leading and trailing edges, nose radius ratio = approximate radius of wing at leading edge/chord, and twist = base to tip twist angle.

Table 2.1: Morphometric parameters for various bird wings [14]

	Length (m)	Projected area (m ²)	Wetted area (m ²)	AR	Thickness ratio	Camber ratio	Nose Radius ratio	Twist (degrees)
Swift	0.141	0.005	0.0104	3.9	0.054	0.054	0.012	5
Petrel	0.212	0.0116	0.024	4.1	0.048	0.065	0.011	9
Woodcock	0.171	0.0137	0.029	1.9	0.053	0.081	0.019	7
Wood duck	0.257	0.0211	0.044	3.1	0.100	0.069	0.020	11
Quail	0.145	0.0109	0.023	1.8	0.036	0.101	0.019	5
Starling	0.164	0.0088	0.035	3.0	0.036	0.112	0.032	13
Nighthawk	0.260	0.0165	0.035	4.1	0.062	0.069	0.035	5
Hawk	0.394	0.0522	0.112	3.0	0.068	0.099	0.032	10
Vulture	0.180	0.00410	0.0086	7.9	0.063	0.039	~ 0	15

Immediate experimental results of the lift and drag coefficients of the nighthawk wing are displayed through **Figure 2.4**. Very similar trends are exhibited in comparison to standard aircraft aerofoils, especially in the parabolic curve of the C_D C_L plot, supporting the argument Withers makes.

Empirical data of lift and pressure drag coefficients as presented by Withers is show

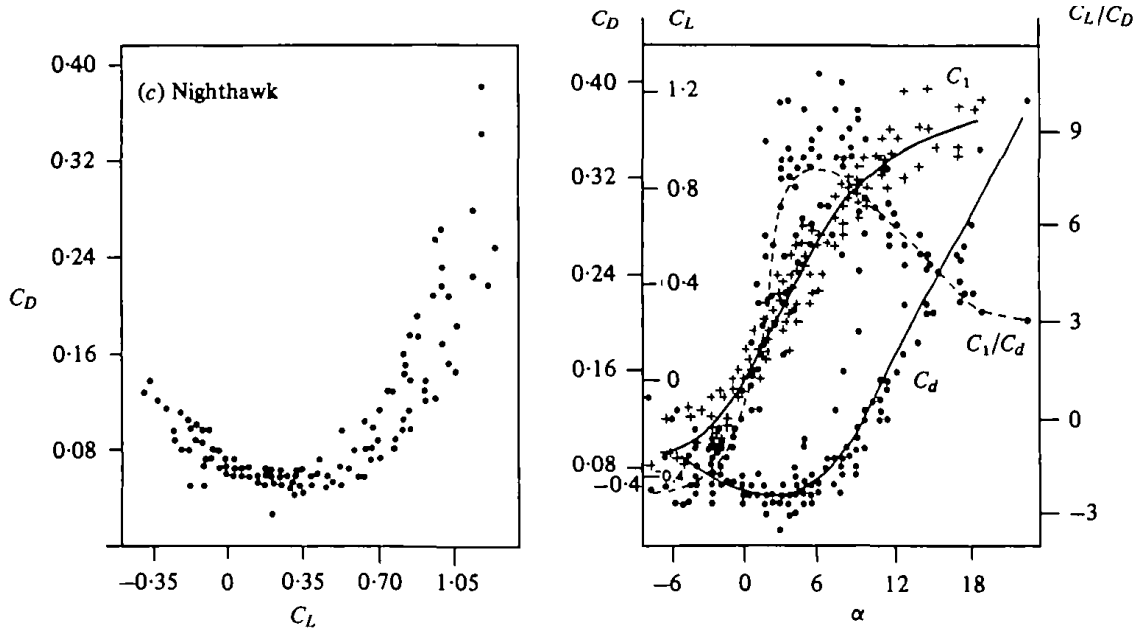


Figure 2.4: Nighthawk Wing. LEFT: lift coefficient (C_L) as a function of drag coefficient (C_D). RIGHT: lift coefficient (C_L), drag coefficient (C_D), and lift/drag ratio (C_L/C_D) at differing angles of attack (α) [14]

through **Table 2.2**. It contains a specific analysis of the nighthawk wing at differing angles of attack (α), with a direct comparison to measured values from the attached force transducers, with an assumed skin friction drag coefficient of 0.02.

Table 2.2: Lift and pressure drag coefficients calculated for the nighthawk wing [14]

	Calculated	Measured	Calculated	Measured
α	C_L	C_L	$C_{D, \text{pre}}$	$C_{D, \text{pre}}$
-8	-0.46	-0.40	0.06	0.08
-4	-0.13	-0.18	0.04	0.06
+2	0.44	0.29	0.03	0.04
+7	0.76	0.60	0.06	0.04
+20	0.66	1.1	0.18	0.28

2.2 Mathematical Background

2.2.1 Lift and Drag Coefficients

Fundamental dimensionless quantities are used to characterise wing and aerofoil performance. The lift coefficient (C_L) and the drag coefficient (C_D) are the most prominent ones used in aerodynamic analyses. Comparison across different conditions is allowed through scaling by normalising lift and drag forces to air density, velocity, as well as characteristic area, which is usually the surface area of a wing in experimental and theoretical analysis [15], [16].

The lift coefficient is depicted through **Equation 2.1**, where L represents the lift force, ρ is the density of air, V is free stream velocity, and S is the wing planform area [15].

$$C_L = \frac{L}{0.5\rho V^2 S} \quad (2.1)$$

Similarly, the drag coefficient can be expressed through **Equation 2.2**, where D is the drag force [16].

$$C_D = \frac{D}{0.5\rho V^2 S} \quad (2.2)$$

Both the lift and drag characteristics over a wing section are either collected through empirical testing or simulated through computation fluid dynamics (CFD). The experimental approach includes wind tunnel testing, which allows for a direct measurement of these coefficients through carefully controlled conditions. This is incredibly valuable for validating aerodynamic theories and especially the credibility of computation solvers [17].

2.2.2 Dimensionless Properties: Reynolds Number

The Reynolds number (Re) is a critical dimensionless parameter which determines the flow regime - laminar, transitional, or turbulent - based on a measure of the ratio of inertial to viscous forces within a given fluid. Defined in **Equation 2.3**, L is the char-

acteristic length (usually the chord length, a straight line measured from the leading to the trailing edge of an aerofoil), V is velocity, ρ is the density of the fluid, and lastly μ is the dynamic viscosity [18].

$$Re = \frac{\rho V L}{\mu} \quad (2.3)$$

Low Reynolds numbers correspond to smooth laminar flow, whilst high Reynolds numbers associate themselves with chaotic turbulent flows [18], [19]. This dimensionless parameter can be altered by changing fluid speed or changing the test section such that conditions closely match up with those in the real world (for scaled models). Schlichting et al. emphasise the importance of matching the Reynolds numbers between real applications and scale-model testing due to it affecting boundary layer behaviour and, therefore, lift and drag forces [20].

2.3 Wind Tunnel

2.3.1 Background of Wind Tunnel Testing

Wind tunnels are a critical experimental tool to analyse aerodynamics through simulating airflow around scale models of wings, aircraft, as well as vehicles [21]. A controlled testing environment is allowed, including aerodynamic parameters such as lift, drag, and pressure distribution - empirical data that aids with design choices as well as validating theoretical models.

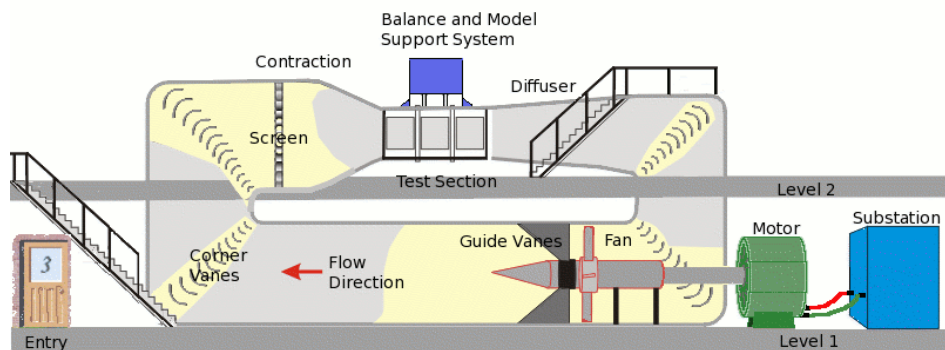


Figure 2.5: Aeromech Wind Tunnel 8m × 10m [22]

Wind tunnels are classified by different flow speed regimes, including subsonic, transonic, supersonic, and hypersonic, all specific to different flight regimes. More focus is delved into the subsonic tunnel due to the facilities the University of Sydney has to offer, as shown in **Figure 2.5**. Accurate measurements require the control of potential sources of error, such as wall interference, turbulence, as well as model blockage effects, which can all affect the quality of data [23].

2.3.2 Boundary Layer and Effects

Walls or bodies have a boundary in which fluid cannot move due to a no-slip condition (friction). This is also known as the boundary layer, which represents this flow region. The boundary layer region has a velocity lesser than the free stream velocity and follows an increasing function from zero at the wall towards the free stream value [24], [25].

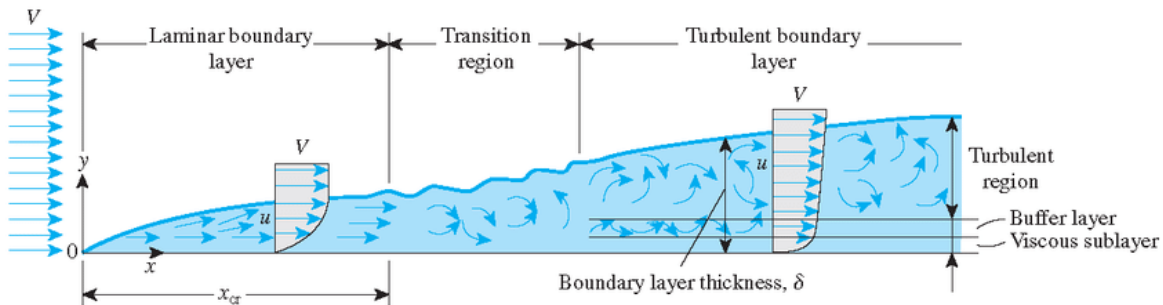


Figure 2.6: Boundary Layer Wall Depiction [26]

As defined by Schlichting, the wind tunnel section can be treated as flow along a flat plate, meaning Blasius' flat plate approximation can be used [20]. Hence, the boundary layer thickness $\delta(x)$ at position x along a surface can be defined as the vertical distance y from the surface where the local velocity $u(y)$ is at 99% of the free stream velocity U_∞ , as shown in **Equation 2.5** [20][25][27].

Mathematically, the local velocity at this thickness can be represented through **Equation 2.4**.

$$u(\delta_{99}(x)) = 0.99 \cdot U_\infty \quad (2.4)$$

This leads into the boundary layer thickness being represented in **Equation 2.5**.

$$\delta_{99}(x) = \frac{5}{\sqrt{Re_x}} \cdot x \quad (2.5)$$

The coefficient $\frac{5}{\sqrt{Re_x}}$ of x represents an empirical factor derived from Blasius' flat plate solution for laminar boundary layers [20][27]. Re_x represents the local Reynolds number, at position x , identical to the one shown in **Equation 2.3**. As such, the effects of boundary layers in the wind tunnel need to be attenuated such that the test model follows the conditions as close as possible to that of free air.

2.3.3 Classical Correction Factors

As mentioned by Edwald et al. in the Advisory Group for Aerospace Research & Development (AGARD), wind tunnels are an enclosed volume which affects the flow properties on a model [28]. Different types of classical correction factors for lift and drag are introduced. This includes **blockage corrections** for “models of unusual shapes” [17], in which the **total blockage factor** ε_t accounts for the ratio of the frontal area of a model to the test sectional area, and is equal to the sum of both **solid** ε_{sb} and **wake blockage** ε_{wb} , shown in **Equation 2.6** [17][29].

$$\varepsilon_t = \frac{1}{4} \frac{\text{model frontal area}}{\text{test section area}} = \varepsilon_{sb} + \varepsilon_{wb} \quad (2.6)$$

Other correction factors include **horizontal buoyancy**, where the boundary layer height has the possibility to increase along the length of the wind tunnel testing section. Lastly, the walls of the wind tunnel have the tendency to correct the **curvature of streamlines** around the model. This could potentially lead to greater lift readings than what actually may be the case in reality [17][28][29].

2.4 Case Studies of Existing Ornithopters

This section particularly focuses on the following, which through the completion of several case studies, will help guide and narrow down a much more specific research pathway for this thesis:

- material usage
- wing mechanism
- manufacturing techniques
- wind tunnel setup and usage
- measured variables

A trade-off is done at the end of this section, comparing the pros and cons of each ornithopter design and outcomes.

2.4.1 RoboFalcon

The RoboFalcon is a bioinspired flapping-wing aerial vehicle (FWAV) designed by Chen et al. [30]. It shows an extremely detailed design, especially mimicking the wingbeat kinematics of flying vertebrates. It utilises bat-styled membrane morphing wings, which, as mentioned before, is essential for agility and efficient flight capabilities, and is shown through **Figure 2.7**.



Figure 2.7: RoboFalcon Ornithopter in Flight [30]

Manufacturing and Material Usage

The RoboFalcon's structure is primarily built using carbon fibre components, which are cut using a Computer Numerical Control (CNC) router to create a frame which exhibits a high strength to weight ratio. The specific material choice helps ensure rigidity, while not being heavy - essential for wing flapping dynamics. Furthermore, the wing membrane is made from an unstretchable polyester fabric to avoid unnecessary energy consumption that would occur due to elastic damping in the wing morphing motion. This seems to be a common issue in bat-inspired designs.

Wing Mechanism

The wing mechanism of the RoboFalcon is relatively complex, with a one degree of freedom (DOF) multilink mechanism that mimics the natural wing morphing seen in bats, pictured in **Figure 2.8**. This includes elements such as:

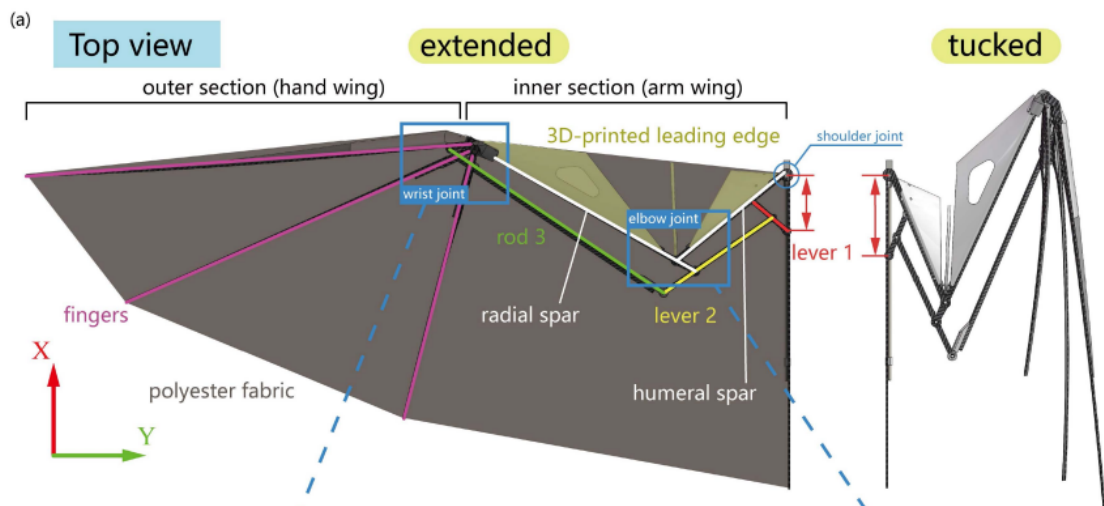


Figure 2.8: RoboFalon Wing Mechanism [30]

- **Lever 1:** Drives the morphing motion, allowing the wings to extend during the downstroke and tuck during the upstroke
- **Wrist joint:** Designed with a pitch-up mounting angle to mimic the natural wrist movements of bats, adjusting passive twist of wing during flight to optimise aerodynamic forces

- **Elbow joint:** Positioned to increase camber of the wing, helps generate extra lift at downstroke stage

Wind Tunnel Setup and Variables

Within the wind tunnel testing section of this study, the RoboFalcon was subjected to a series of experiments to measure lift, thrust, power consumption, and rolling moments under a variety of different wing configurations. These tests were essential to understanding the effects of different morphologies on aerodynamic performance. Key findings from RoboFalcon's wind tunnel tests include:

- **Wrist mounting angle:** The adjustment of the wrist joint angle significantly impacts the angle of attack, lift and thrust configuration, and power consumption, highlighting how small changes in wing morphology can influence overall flight dynamics.
- **Rolling moment:** The asymmetric downstroke enabled by the morphing wings is highly effective in roll control efficiency. There is a high correlation between flapping frequency and rolling moment, with higher flapping frequencies improving the rolling capabilities.

2.4.2 Korean Bioinspired Ornithopter

Lee and Han (2012) of the Korean Department of Aerospace Engineering faculty conducted an experimental study on a bioinspired ornithopter to understand the complex principles of flapping wing flight [31]. Their research involved free flight and wind tunnel testing procedures. What was unique about their approach, was their use of a 3D visual tracking system to capture the oscillatory behaviours and aeroelastic deformations of the wings and tail, shown through **Figure 2.9**.

Manufacturing and Material Usage

As the paper itself does not focus on the manufacturing process, the detailed material usage is not outlined. However, it is mentioned that the ornithopter utilises lightweight and flexible materials to mimic the natural aeroelastic characteristics of insect wings.

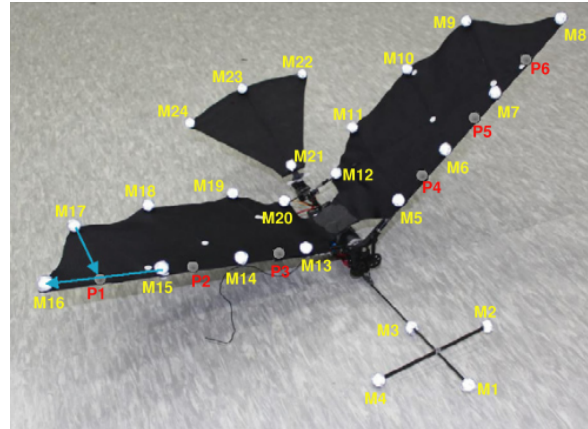


Figure 2.9: Korean Bioinspired Ornithopter with Visual Trackers [31]

This meant the use of anisotropic flexible wings, helpful for generating the necessary forces and moments.

Wing Mechanism and Flight Testing

Pitch stability was a factor that was focused on, hence the feature of wings that could actively rotate to enhance stability. Flexibility within the wings allowed for a passive method of mitigating pitch disturbances, essential for flight stability in a variety of different aerodynamic conditions. Free flight tests conducted also showed the ornithopter undergoing limit cycle oscillations (LCO). This behaviour suggests stability; however, oscillatory flight dynamics within steady conditions.

Wind Tunnel Setup and Variables Measured

A specially designed tether system was used within the conducted wind tunnel tests to mimic free flight conditions, whilst lessening the impact of mechanical interference. This allowed a series of controlled pitching moment disturbances to be added to the system to test ornithopter stability. There was a specific focus on measurements, including body pitch angles, tail movements, as well as wing/tail interaction dynamics, as shown in **Figure 2.10**.

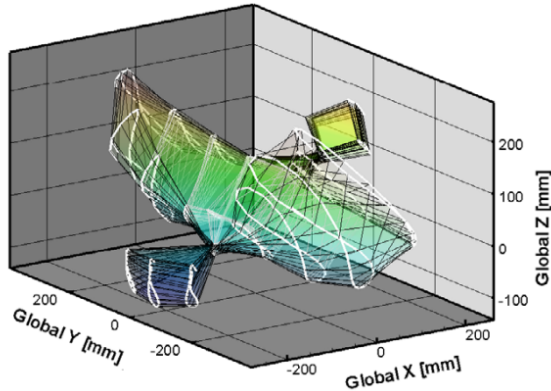


Figure 2.10: Global Wing, Tail, and Body Trajectories of Marker Sets [31]

Active Tail Motion

A significant portion of the study was the introduction of active tail motion to mitigate the magnitude of LCOs during flight testing. Changing the tail's movement together with the wings helped enhance longitudinal stability. This is essential for smoother flight as it could lead into more practical ornithopter applications, including surveillance and reconnaissance missions where stable and controlled flight is of high importance.

2.4.3 Scibilia and Wojciechowski Model

The study conducted by Scibilia and Wjciechowski (2006) focuses on comparing experiments between ornithopter and plane models to understand aerodynamic behaviours under simulated conditions [32]. Wind tunnel testing is done to test different surface treatments and vibrational forces on the aerodynamic properties of these models.

Manufacturing and Material Usage

The ornithopter developed in this study is built with two rigid wings of a Clark Y aerofoil profile, of 20cm wing span. This specific aerofoil features a nearly flat lower surface and a moderately cambered upper surface. Although material choice is not specified in detail, it is mentioned that they are rigid enough for wind tunnel experiments, especially to be flapping at the designated frequencies.

Wing Mechanism and Flight Testing

The mechanical wing flapping mechanism is actuated by a crank and gear system, as powered by an electric motor. Longitudinal axis flapping (ϕ) is achieved, as well as feathering around the wing axis (ψ), shown through **Figure 2.11**. This results in two DOF, which helps with mimicking bird wing motion. The only issue of this study is that it utilises a rigid wing, and does not exhibit wing morphing characteristics. A total flapping angle of 40° is achieved at a frequency of 5 Hz, in accordance with feathering angles between $\pm 10^\circ$ and $\pm 20^\circ$. Wind tunnel velocity ranged from 8 to 16 m/s, which corresponded to Re 42000 - 85000.

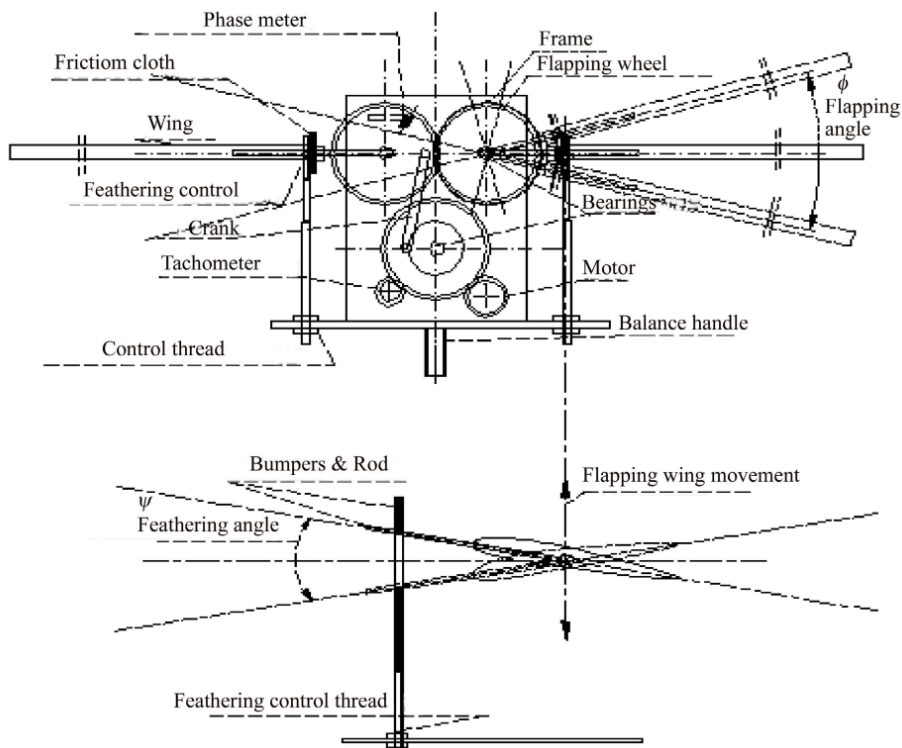


Figure 2.11: Moving Wing Mechanism and AOA Control (Scibilia et al. 2006 [32])

Wind Tunnel Setup and Variables Measured

Wind tunnel testing required that the ornithopter is secured on a balance to measure lift and drag forces. Both static and dynamic tests were conducted, with the dynamic measurements within phase positions of the wings. This ultimately helped with exploring the aerodynamic effects on the ornithopter at varied flapping and feathering

angles. A great deal of focus is on how the forces change over a number of flapping cycles, which sheds more light into aerodynamic sensitivity in a parametric study. A 5-multicomponent strain gauge balance was used for the dynamic measurements.

Key Findings

The main takeaway from this specific study is that lift and drag are highly dependent on Re , wing flapping amplitude, as well as the interplay between flapping and feathering. This interaction between each other significantly influences the efficiency associated with lift generation and drag reduction, providing insight into ornithopter performance optimisation.

2.4.4 MEMS Wing Ornithopter

Pornsin et al. presents a detailed study into the development of a Micro Aerial Vehicle (MAV) ornithopter with Micro Electro Mechanical Systems (MEMS) wings [33]. The project's goal was to create a battery-powered ornithopter that combines lightweight design with effective aerodynamic properties, especially testing within a calibrated low speed wind tunnel.

Manufacturing and Material Usage

Materials used to build this ornithopter were selected to satisfy the design requirements of <15cm wingspan. As such, the wing frame uses a titanium alloy metal due to its high strength to weight ratio, and its fabrication process is shown through **Figure 2.12**. The membrane itself was manufactured using parylene C, especially for its properties of adhesion to titanium alloy and its durability under high wing flapping frequency - up to 30 Hz without breaking. In addition to these materials, different permutations are also developed using paper, mylar, as well as carbon rods to measure aerodynamic performance.

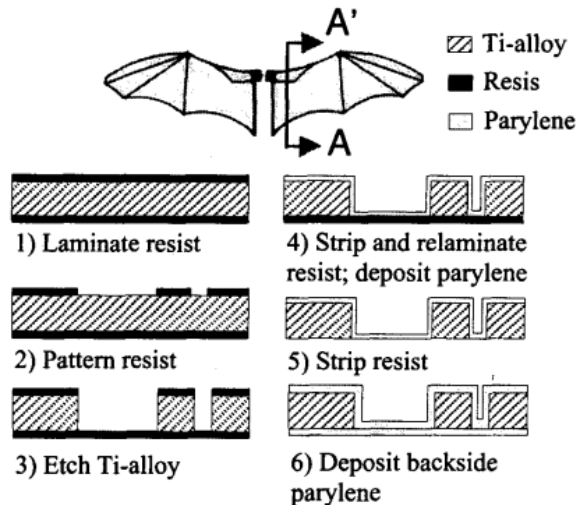


Figure 2.12: Fabrication Process of Titanium Alloy MEMS Wings [33]

Wing Mechanism and Flight Testing

The wing itself also does its best to mimic ornithopter morphology through flapping and feathering motions.

Wind Tunnel Setup and Variables Measured

Wind tunnel testing for this ornithopter included a velocity uniformity of 0.5%, with air speeds ranging from 1 m/s to 10 m/s. The focus of this was to see how different wing configurations influenced lift, drag, and overall flight efficiency. Measurements included the tracking of lift and thrust generation across different wingbeat amplitudes and frequencies, giving a good understanding of performance under controlled circumstances.

2.4.5 Srigrarom and Chan Model

This study by Srigrarom et al. focuses on the development and configurations of an ornithopter prototype and analyses the effects on aerodynamic performances based on different wing designs [34]. This specific case study will be sectioned slightly differently, focusing on each individual prototype.

First Prototype

The first prototype of the Srigrarom and Chan model is shown through **Figure 2.13**.

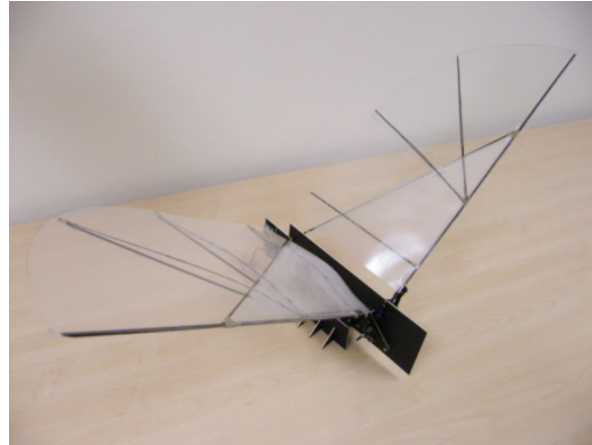


Figure 2.13: Srigrarom and Chan First Prototype Ornithopter [34]

- **Material and Design:** Used carbon rods and ripstop fabric, chosen for durability and lightness, typically used in kites. This combination, however, was too heavy, which impacted ornithopters to generate enough lift
- **Flapping Mechanism:** The initial flapping mechanism lacked efficiency and synchronisation, leading to subpar aerodynamic performance
- **Challenges:** Overall weight and inefficient flapping mechanics, did not allow for sustained flight

Second Prototype

- **Design Adjustments:** Modifications were made to reduce weight and improve upon flexibility. The structure was refined to better accommodate aerodynamic stresses when flapping
- **Material Upgrades:** Wing material switched to lighter material Orcon, allowing for better wing flex
- **Performance:** Improvements in the lift were noted; however, there were continual issues with thrust consistency and structural durability

Third Prototype

The final prototype consists of using carbon as their main structural element, as shown through **Figure 2.14**.

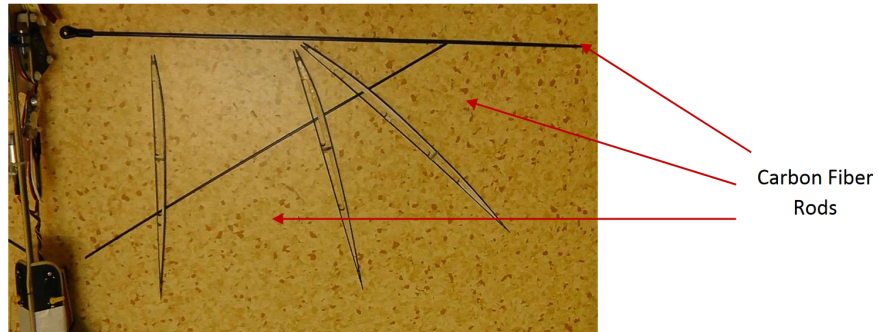


Figure 2.14: Srigrarom and Chan Model Wing Skeletal Structure [34]

- **Advanced Manufacturing:** 3D printing used for precise construction of wing frame, allowing for further weight reduction and specific geometries
- **Wing Mechanism:** Introduced a more sophisticated flapping mechanism that leveraged near-resonance phenomena for more effective wing movement, enhancing lift and thrust. The maximum flapping frequency achieved was 3.869 Hz, with 0.719 N lift and 0.264 N thrust

Wind Tunnel Testing

A force balance made of load cells was used to measure lift and thrust forces within the tunnel. At three different speeds of slow, medium, and fast, the lift was measured over ten wingbeat cycles to calculate average lift and frequencies, as shown through **Figure 2.15**.

2.4.6 FESTO - SmartBird

Through a white paper produced by FESTO - Smart Bird [35], the researchers behind the ornithopter detail advanced mechanisms, including active torsion as well as flying locusts' wing kinematics. The successful design of this led to an extremely elegant flight mechanism, as demonstrated through their YOUTUBE video. Figure

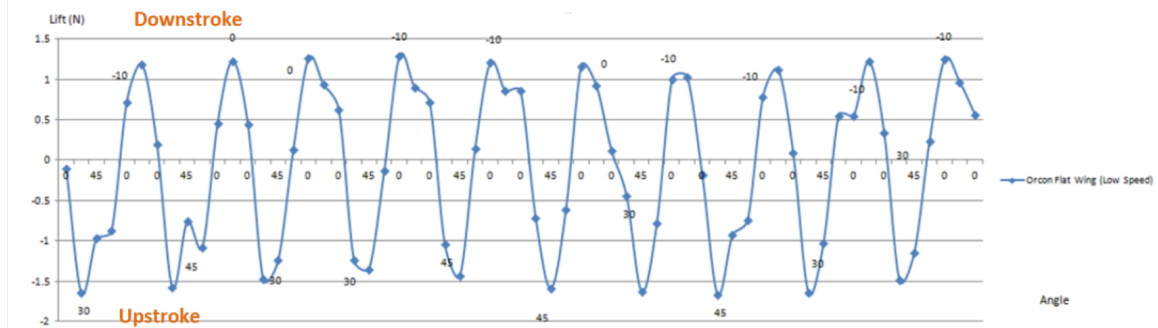


Figure 2.15: Average Lift Force vs Flapping Angle [34]

Figure 2.16 shows the in-depth view of the front of the SmartBird. The breakdown of key components and methods is shown in the following sections.

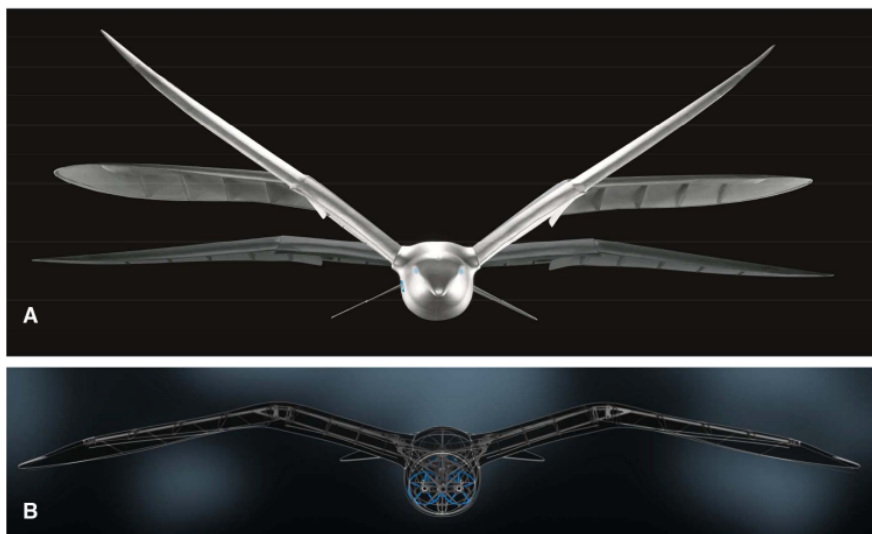


Figure 2.16: Front View (A) and X-Ray View (B) of FESTO SmartBird [35]

Manufacturing and Material Usage

As mentioned in the paper, FESTO features a “lightweight design integrating high-tech materials and components” [35]. The main material that is used is primarily carbon fibre for its body and wings, which, similar to other ornithopters, ensures a great strength-to-weight ratio for the best aerodynamic properties.

Wing Mechanism

The wing mechanism of FESTO uses a wing spar configuration contained in two main parts:

- **Inner wing spar:** functions to generate lift
- **Outer wing spar:** aids in thrust generation, connected through a trapezoidal hinge. The hinge mechanism has a 1:3 transmission ratio for flapping efficiency.

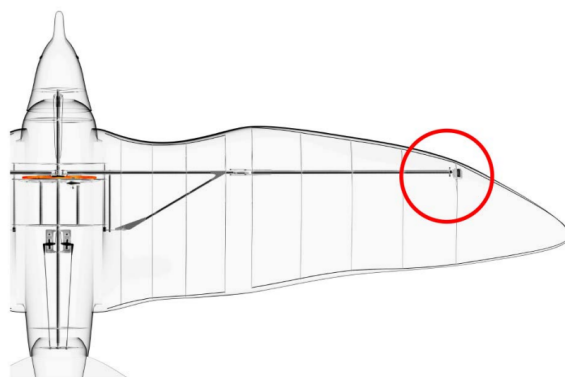


Figure 2.17: Top View of FESTO Wing and Torsion Motor Sensor [35]

Furthermore, as mentioned earlier, active torsion is used on FESTO, shown through **Figure 2.17**. This is achieved through a servo motor located at the wingtip, adjusting the angle of the wing through each flapping cycle to enhance aerodynamic efficiency. The ability to switch between a positive angle of incidence to a negative one improves both lift and thrust.

Wind Tunnel Setup and Variables Measured

The wind tunnel experiments were aimed at measuring and optimising the aerodynamic properties of FESTO. It mainly focused on adjusting flapping frequency and amplitude, analysing their effects on lift and thrust.

2.4.7 Summary of all Case Studies and Contributions

Table 2.3 shows a complete yet simplified summary of the comparison between the six case studies analysed. Core themes such as manufacturing, material, wing mechanism, wind tunnel usage, and measured variables are looked at specifically.

Table 2.3: Comparative Analysis of Ornithopter Models

Ornithopter Model	Manufacturing and Material	Wing Mechanism	Wind Tunnel Setup and Usage	Measured Variables
RoboFalcon	Carbon fiber, CNC routed; polyester wings.	Multilink, one-degree of freedom, bat wing morphing.	Lift, thrust, power, rolling moments tested under various configurations.	Lift, thrust, power, rolling moments.
Korean Bioinspired Ornithopter	Lightweight, flexible materials; anisotropic wings.	Active rotation for pitch stability; passive disturbance buffering.	Tether system to mimic free flight; controlled disturbances introduced.	Body pitch angles, tail movements, wing/tail dynamics.
Scibilia and Wojciechowski Model	Rigid Clark Y profile wings; wind tunnel durable materials.	Crank and gear system for flapping and feathering.	Balance secured; static and dynamic tests.	Lift and drag, flapping and feathering impacts.
MEMS Wing Ornithopter	Titanium alloy frame, parylene C membrane; variations with other materials.	Natural flapping and feathering motions for high-frequency flapping.	Low-speed tunnel, 1 to 10 m/s; various wing configurations tested.	Lift, drag, flight efficiency; impact of wingbeat amplitudes and frequencies.
Srirarom and Chan Model	Carbon rods, ripstop, later Orcon for lighter wings.	Advanced flapping mechanisms leveraging near-resonance phenomena.	Load cells measure lift and thrust at varying speeds.	Lift and thrust across speeds; wingbeat frequency impacts.
FESTO - SmartBird	Carbon fiber for body and wings, high strength-to-weight.	Wing spar configuration with active torsion via trapezoidal hinge.	Focus on optimizing flapping frequency and amplitude.	Aerodynamic properties, lift and thrust effectiveness.

2.4.8 Proposed Solution

Based on the comparative analysis of the six different ornithopter models as shown in **Table 2.3**, a narrowed-down solution is now proposed to further the research objective of this thesis. Using a hybridised approach of carbon fibre rods and flexible polymers such as parylene C or ripstop fabric will ensure the best of both words in terms of strength to weight, and aerodynamic flexibility.

Manufacturing techniques such as 3D printing within the University of Sydney's Fabrication Laboratory (FABLAB) will be leveraged for its precision, quick turn-around time, as well as custom wing geometries. This 'frankenstein' framework will be validated through comprehensive wind tunnel testing, with a focus on rapid iterations through available resources. With respect to the University's wind tunnel, load cells will be used to measure lift and drag, contributing to a complete parametric study that is to be done to achieve a whole data map of values. Ultimately this can be used as empirical data as a form of validation for **Victor Zhou's blade element solver** regarding pitching and heaving motions.

This page is intentionally left blank.

Chapter 3

Methodology

3.1 Wing Kinematic Design

As mentioned in the literature review from the Chapter beforehand, the case studies' designs do not explore 'true' flight styles, including nature's tucking and morphing aspects. Hence, the kinematic design of the wing for this thesis follows a bio-inspired pathway. Potential benefits could also be seen from tucking, as also touched on in literature. Due to the difficulty in replicating the material of feathers, a bat-styled wing design is employed. Hedenstrom et al. mention several similarities between the lift generation between birds and bats. However, bat flight is more suited for low-speed characteristics [36]. It is also mentioned that a primary difference between the two is the structure of the wings. Birds manoeuvre through the air by changing the shape of their feathers, effectively correcting camber and pressure differences between top-side and bottom-side surfaces [36]. On the other hand, bats have longer finger bones (phalanges), which hold the skin membrane (patagium) and allow it to stretch outwards, creating a lifting surface. [37].

The representation of bird and bat platforms is shown in **Figure 3.1**.

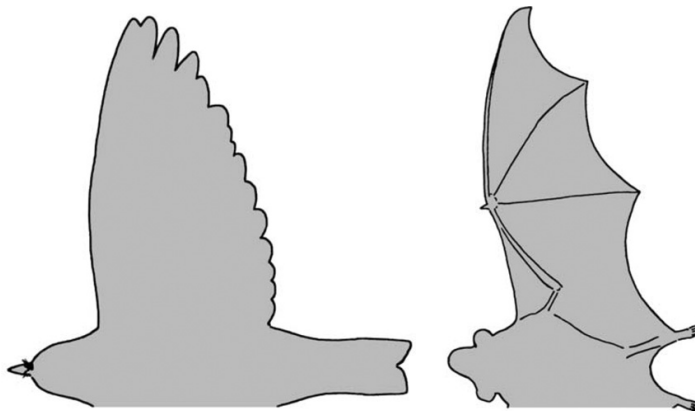


Figure 3.1: Wing semi-span planform view, LEFT: small passerine bird, RIGHT: Pall's long-tongued bat [36]

3.1.1 Bio-inspiration

Bio-inspiration is the core of many engineering feats, including the modern Japanese bullet train ‘Shinkansen’, which was based on the pointy beak of a kingfisher bird to aid in more streamlined fluid behaviour [38].

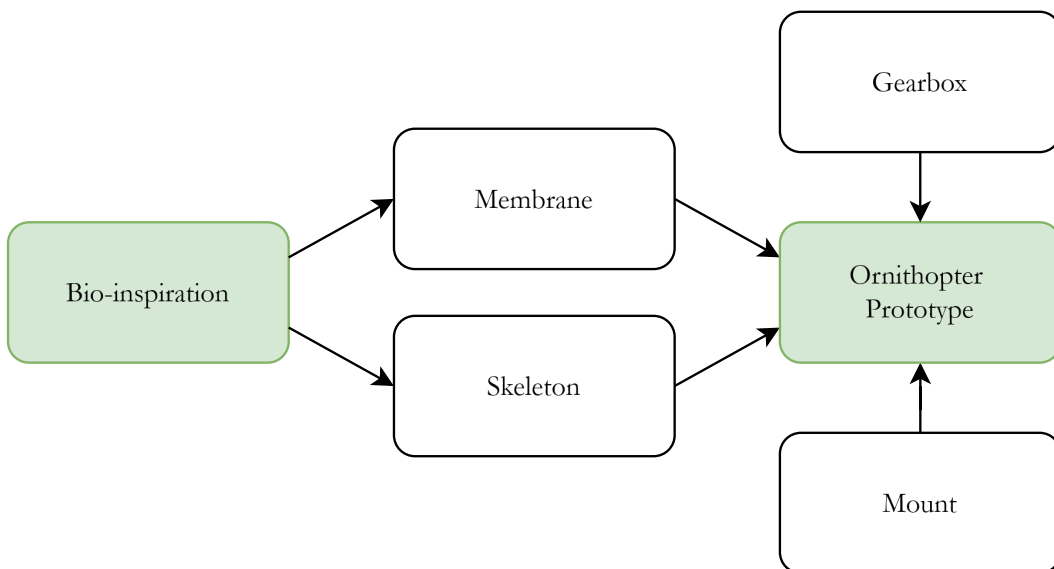


Figure 3.2: Ornithopter Design Architecture

The overall design architecture is divided into four contributing sections: the skeleton, membrane, gearbox, and mount. A more graphical representation of this is shown in **Figure 3.2**.

For the objectives of this thesis, a bat-styled wing is designed based on the dimensions

of the wind tunnel testing facility and the manufacturing methods available. Due to the lack thereof in literature, the tucking behaviour is focused on as a significant design point. The source of inspiration can be quantified by a single image, as shown in **Figure 3.3**. From the fur on the left begins the shoulder, leading into the elbow joint, then the wrist joint, which stems into three main fingers [39].



Figure 3.3: Photograph of the underside of a bat wing [40]

3.1.2 Computerised Design

One of the final wing skeletal designs achieved on Computer-Aided Design (CAD) is shown in **Figure 3.4**. What is shown clearly is the shoulder, elbow, and wrist joints, which contain three fingers. Also portrayed in **Figure 3.4b** and **Figure 3.4a** on the left-hand side is a slide mechanism which allows the skeleton to extend from the tucked position. Note that this design is inspired and modified from that in Robofalcon, as designed in 2022 by Chen et al. [30].

This particular design has taken the manufacturing constraints into deep consideration. With access to 3D printers and laser cutters, members shown in **Figure 3.4** needed to contain as little bridging as possible (3D printing), as well as not containing internal designs since it is not accessible (laser cutter). Conveniently, another design consideration was the weight of the skeletal linkages, which, because of acrylic and plastic 3D printing material, helped achieve this.

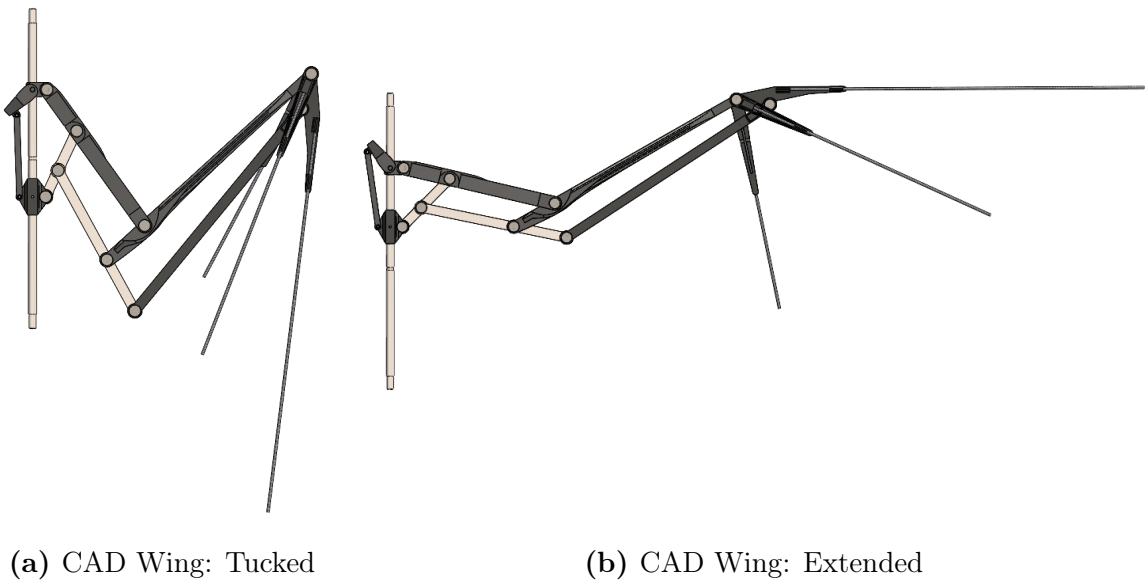


Figure 3.4: Wing skeleton in CAD, Choudhury [41]

3.2 Material Properties and Choices

3.2.1 Material Selection Overview

One main objective of material selection was to replicate the bio-inspired wing design so that it could undergo cyclic aerodynamic forces for both static and dynamic testing. Some key criteria to satisfy this objective included the following:

- **Strength to weight ratio:** Materials must be strong yet lightweight, minimising extra mass that could impact aerodynamic performance.
- **Fabrication precision:** Several components required precise dimensions, such as connectors, supports, and especially gear components, were designed and chosen depending on their compatibility with 3D printing, laser cutting, and machining.
- **Flexibility and Durability:** Flexible materials were essential for the wing membrane to simulate the dynamic responses of biological wings without sacrificing structural rigidity, primarily through repeat load cycles.

This specific approach allowed materials compatible with available manufacturing tech-

niques offered through the University's resources.

3.2.2 Material Descriptions

- **PLA (Polylactic Acid):** PLA was selected as a primary material for 3D printed parts due to its relative rigidity, accessibility in the lab space, and ease of use. Research supports PLA's precision in applications requiring structural but low load-bearing parts, including connectors and frame supports [42].
- **Acrylic:** Acrylic was chosen for gears and other relatively rigid structural supports. These were selected because they required higher tolerance precision, especially with the gear teeth profiles. Acrylic's rigidity and low weight do indeed help with the stability of the frame. However, it is more brittle under impact [43]. Hence, its role is relatively limited in dynamic areas.
- **Carbon Fibre Rods:** Carbon fibre has a high strength-to-weight ratio [44] and is, therefore, the best material to handle cyclic loading while flapping. It is frequently used in aerospace due to its stiffness properties and minimal deformation under stress [45]. Because of these ideal material properties, it does become more costlier, which will be beneficial for critical load-bearing parts.
- **Nylon Ripstop Fabric:** Ripstop fabric is a type of interwoven material through long nylon strands [46]. This material is more often used in camping gear and is also well known for its use in the manufacture of parachutes [47]. The material's resistance to tearing [48] also leads to further use in parachute recovery systems. It also has low permeability [49], making its use as a wing membrane an excellent contender.
- **Nylon 3D Print Filament:** Nylon printed filament provides low friction and is resistant to high temperatures [50]. Because of this material property can also be used as gears, as shown by Muminovic et al. [51]. Metal gears would be much preferred; however, due to manufacturing constraints, nylon filament is the most welcoming option.

Material Trade-off Analysis

To summarise the justifications in the previous section, a simple trade-off study is shown in **Table 3.1** and aligns each material in accordance with this thesis' requirements.

Table 3.1: Summary of Material Trade-Offs

Material	Strength-to-Weight Ratio	Durability	Precision & Ease of Manufacturing	Cost	Primary Use
PLA	Moderate	Moderate	High (easy to 3D print)	Low	Non-load-bearing connectors, frames
Acrylic	Moderate	Moderate	High (laser cutting precision)	Low	Rigid structural supports
Carbon Fibre Rods	High	High	N/A (COTS ¹)	High	Wing skeleton fingers
Nylon Ripstop Fabric	Low	High	N/A (COTS ¹)	Mid	Wing membrane
Nylon (Filament)	Moderate	High	Moderate (3D printable, high temp)	Mid	Precision/durable components

¹ COTS stands for Commercial Off-The-Shelf components, purchased as displayed

3.3 Manufacturing and Assembly

This section focuses on manufacturing the flapping wing and assembling all components to satisfy the objectives of this thesis.

3.3.1 Fabrication Techniques and Justifications

All three-dimensional (3D) printed models in this thesis were created through the University's Fabrication Laboratory (FabLab). The NUPBOX printers operate through pre-programmed G-code through a Cartesian axis using a Fused Deposition Method (FDM). The printers themselves have a 0.2 millimetre nozzle, which extrudes PLA at 210° Celsius. To attenuate the warping of the printed part, the print bed is set to a temperature of 60° Celsius, ensuring optimal printing quality [52]. As the nozzle is 0.2 millimetres thick, each layer of print height is also inherently 0.2 millimetres. All these print settings ensure a high-quality finish with decent accuracy.

Another manufacturing technique employed was the Epilog Fusion M2 laser cutter. Due to the material in FabLab, acrylic pieces were designed to have thicknesses of

either 3 or 6 millimetres. This process uses a high-powered carbon dioxide laser to cut non-metallic material [53]. Like the 3D printers, the laser cutter uses a Cartesian-styled system for vector cutting. The settings for 3 millimetres of acrylic include 100 Hertz as the frequency, 10% speed, and 100% power, whilst the 6 millimetres of acrylic requires 3% speed instead. Following these settings provides the best and most accurate finish.

Wing Manufacturing

The manufactured wing is shown in **Figure 3.5**, where each component is labelled.

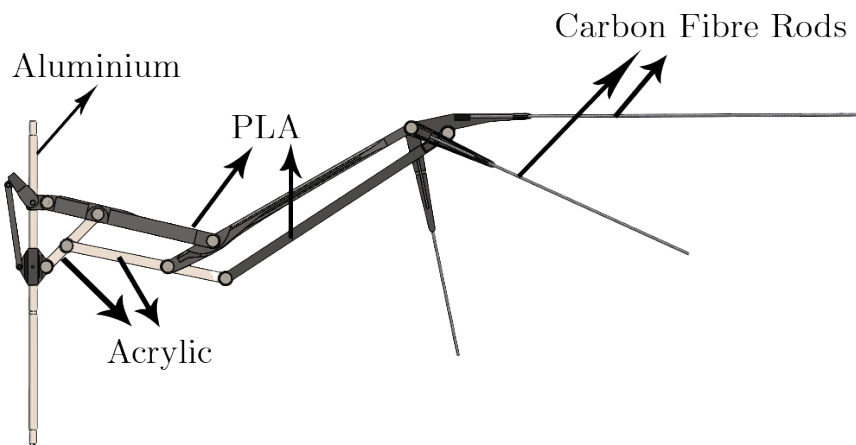


Figure 3.5: Labelled Wing Skeleton Materials

From the left, an aluminium 6061 rod is machined into the shaft as pictured and helps with the rotation mechanism by flapping up and down. Since this is the root of the wing, it holds all of the inertial forces and weight caused by the other components of the wing and must, therefore, be load-bearing and strong. A smooth finish is ensured, as there is also a sliding mechanism, which, as aforementioned, allows the novel tucking motion of this system to occur. Attached to this are acrylic arms, which are simple yet effective. The elbow consists mainly of PLA, due to their slightly more complex geometry, hence going with the 3D printed route. This is due to these parts being load-bearing components. Not only do they undergo compression and tension, but they also undergo bending stresses. To counteract the effects of these stresses, the cross section was designed such that it had an increased second moment of area. Lastly, carbon

fibre rods are used due to their strong yet flexible capabilities as the fingers. This design choice essentially helps absorb the stresses experienced throughout the entire body because of its inherent elasticity.



Figure 3.6: Close up of wrist joint design

The rods are cut to size based on the batwing shown in **Figure 3.3**, used as the main source of bio-inspiration. It is also important to note that all linkages pivot around small three millimetre shoulder bolts, which have been threadlocked with Loctite, thus preventing them from backing out and causing the model to fall apart.

Figure 3.6 highlights the design of the wrist, showing how the carbon fibre rods are integrated as the fingertips.

Wing Membrane

Watching hang gliders launch themselves off the Bald Hill of the Royal National Park revealed a potential lightweight yet strong fabric for aerodynamic purposes, as pictured in **Figure 3.7**. This inspired the design choice for the membrane of this thesis' wing.

After further investigation into nylon Ripstop fabric, its low permeability characteristics [49] are perfectly suited as the membrane. **Figure 3.8** shows the design choice of wrapping the fabric around the skeleton, creating a double layer of membrane, hence further decreasing the total permeability of the material,

The mounting choice for such a fabric was to be sewn onto the skeleton. However, the sewing points needed to be strategically done, or else the dynamic motion of the wing



Figure 3.7: Hang Gliders, Royal National Park

would be restricted. Upon further inspection of the bat wing shown in **Figure 3.3**, the fabric was sewn around each fingertip (carbon rod) and pulled taut to create tension whilst in the extended configuration. Anchoring the other side of the root of the wing, the fabric is sewn onto the aluminium shaft. It was also noticed that even after sewing a perimeter around the entire wing, pockets of air would cause the membrane to balloon. Hence, further sewing reinforcement to the centre areas of the fabric was done to ensure the fabric acted as a single homogeneous layer. The final membrane containing the manufactured skeleton is shown in **Figure 3.9**.

Gearbox Manufacturing

The full gearbox designed by Choudhury [41] accommodates two wings, one on each side. It is modified from this configuration to only hold one wing, such that the other side can be mounted. A flat plate design to lock onto the modified gearbox is also 3D printed and is attached to the load cell side. Within the gearbox, it contains 5 different gears, each contributing to the gear ratio. As pictured in **Figure 3.10**, the gearbox consists of a worm gear directly attached to the motor, which then actuates the first, second, third, and main gears. The wing is directly attached to the main gear and the reduction in gear ratio helps in increasing the torque. The larger gears shown are 80



Figure 3.8: Fabric and Skeleton Integration

teeth spur gears, whilst the smaller ones have 40 teeth. This results in a gear ratio of 160 to 1, where 160 revolutions of the worm gear spin the main gear by 1 revolution.

It is notable to mention that the first, second, and third gears are all laser cut using 3 millimetre acrylic due to their simplicity. The main gear, due to its ball joint housing, can only be 3D printed. No loss of accuracy is seen with 3D printing the gear teeth. Lastly, the worm gear underwent a few iterations, initially 3D printed using PLA. It was found that the high-speed spinning and constant grinding with the first gear caused it to melt and wear out extremely quickly. The solution was to apply multi-use synthetic oil as a lubricant, which helped a great deal. However, the PLA would still melt, so high temperature nylon filament was used instead. It yielded a better print quality and was resistant to the heat generated through friction, ensuring a smooth transfer of torque between the gears. The lubricant was added just as a further precaution.

Due to its relatively complex geometry, the gearbox housing was also 3D printed using PLA. It has to have holders for all the gears and counterbored holes for bolts, as opposed to many laser-cut components all slotting together. It also contains holes of good enough tolerance to have press-fit COTS bearings.



Figure 3.9: Full Membrane Integration

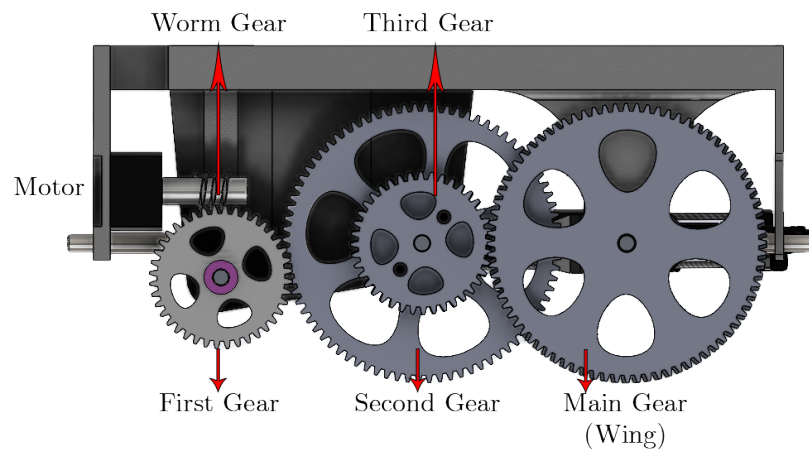


Figure 3.10: Gearbox Inner Mechanism

Furthermore, the bearing shafts were machined out of 6 millimetre brass rods on a lathe and are pictured in **Figure 3.11**. Radial ball bearings are used on each side of the shaft to ensure that the gears spin smoothly. The shafts are also designed with grooves so circlips can lock it in place and prevent it from sliding out of the housing.

Mount Manufacturing

The mount is essential to this thesis as it is the member that connects the test subject to the measurement device. As shown through **Figure 3.12**, the mount's top side contains four bolt holes to attach to the overhead balance. The bottom has a triangular hole pattern to hold the load cell attachment plates. As only the bottom portion protrudes

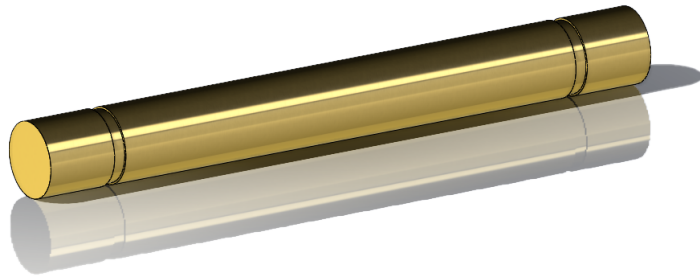


Figure 3.11: Spur Gear Brass Bearing Shaft

into the wind tunnel, it is designed to be an aerodynamic shape as opposed to a bluff body to minimise drag. **Figure 3.12a** shows the airflow direction and the aerodynamic leading edge, as the gearbox is mounted beneath. Moreover, an H-beam inspired design is implemented into the cross-section of the mount, as displayed in **Figure 3.12b**. This mitigates bending stresses due to an increased second moment of inertia and aids in transferring aerodynamic force readings to the load cell as opposed to absorbing the energy.

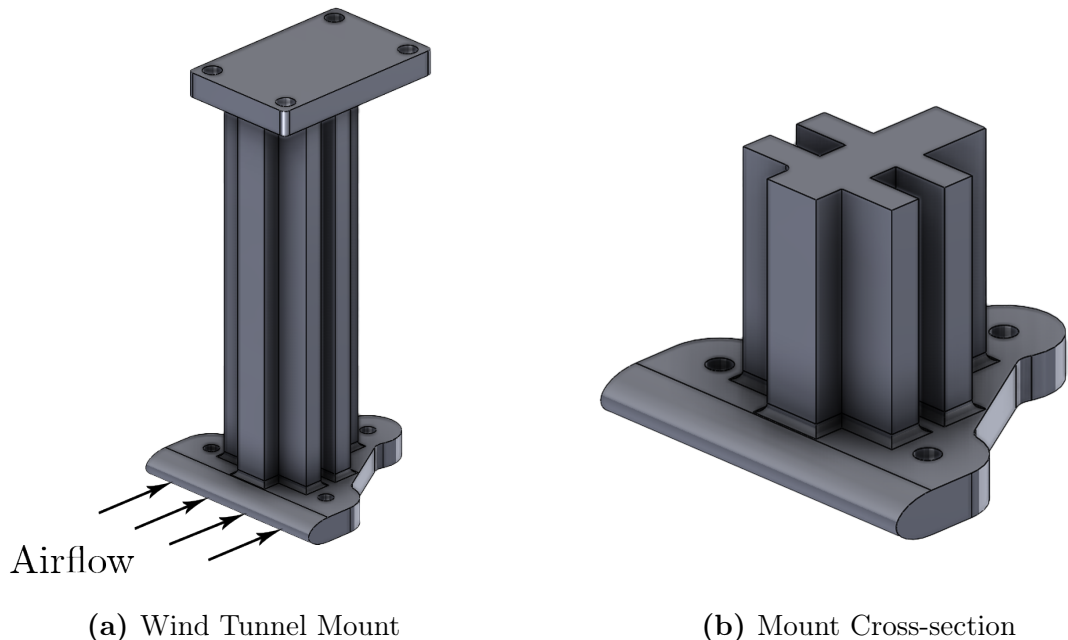


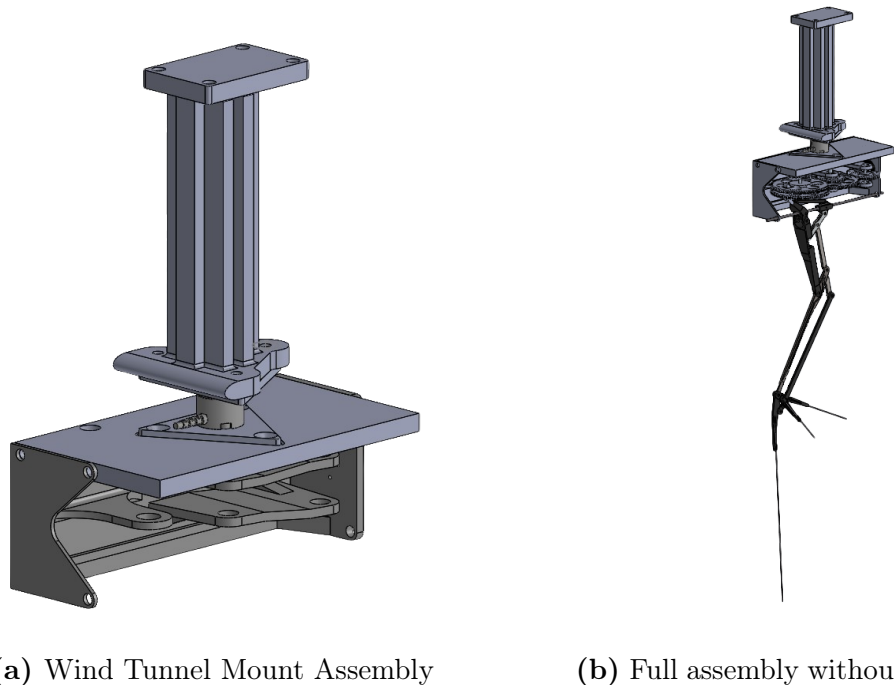
Figure 3.12: Wind Tunnel Mount Design

Similar to the gearbox, this mount was also 3D printed due to its complex geometries.

However, to increase its strength and prevent it from bending, 100% infill was used to make the mount a fully solid block of PLA.

3.3.2 Assembly

Finally, the assembly stage involves piecing all the aforementioned components. **Figure 3.13a** shows a fully integrated design of the single-wing gearbox housing and the mount, encapsulating the load cell between. The four-hole side of the mount is directly bolted to the overhead balance, whilst the wing points downwards.



(a) Wind Tunnel Mount Assembly

(b) Full assembly without membrane

Figure 3.13: Rendered Assemblies

A more intricate assembly of the gearbox, fully assembled, is highlighted through **Figure 3.14**. It contains the aluminium sliding rod for the tucking motion of the wing, the 3D printed PLA and laser cut acrylic gears, as well as the nylon printed worm gear which is attached to the motor. Keeping the spur gears in place are the brass shafts, which are held in place by the circlips.

The complete wind tunnel set-up of all components is shown in **Figure 3.15**, all ready to run.

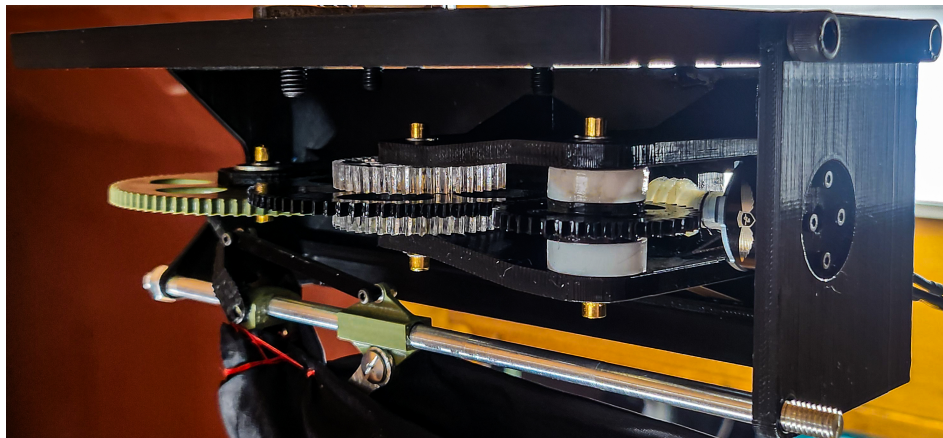


Figure 3.14: Full Gearbox Assembly



Figure 3.15: Complete Wing Setup in Wind Tunnel

Chapter 4

Wind Tunnel Methodology

4.1 Wind Tunnel Preparation and Setup

This section mainly concerns the methodology post-manufacturing, however, immediately prior to the testing stage. It covers the wind tunnel and measurement devices, such as the load cell, in detail.

4.1.1 Wind Tunnel Specifications

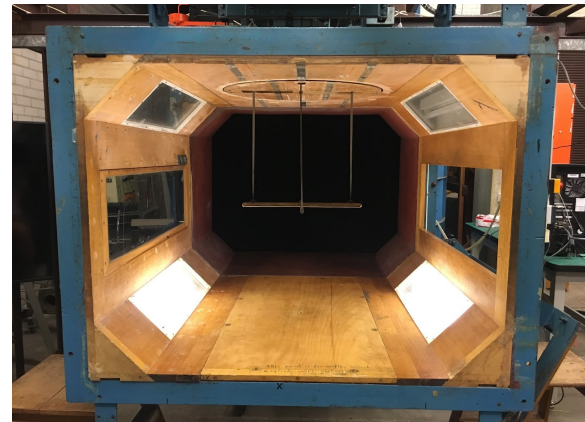
The experimental apparatus used is the University of Sydney's low-speed wind tunnel, which is a closed circuit. The test section, which can be dragged out by sliding rails shown in **Figure 4.1a**, has dimensions of 3 feet wide (1.22 metres) by 4 feet tall (0.91 metres), which also contains corner fillets of 0.5 feet (0.15 metres) by 0.5 feet (0.15 metres), as well as a length of 4 feet [22][54]. As a result, this resembles an octagonal cross-section, depicted in **Figure 4.1b**. Furthermore, the wind tunnel's operating speeds range from five metres to sixty metres per second; however, for the purposes of this thesis only the lower quartile of speeds will be used.

4.1.2 Test Section Setup

A render of the test section setup is shown in **Figure 4.2a**, with a side view in **Figure 4.2b** for added perspective. As can be seen, the single wing and gearbox are



(a) Wind Tunnel External View [54]



(b) Cross-sectional View of Wind Tunnel [22]

Figure 4.1: USYD Low Speed 4×3 feet Wind Tunnel Specifications

mounted pointing downwards, giving space for the wing's dynamic movement. The entire unit is mounted to the overhead balance, essentially locking it in place. Moreover, the balance's angle can be remotely controlled and changed, making testing the angle of attack of the wing much more accessible as opposed to manufacturing different load cell plates.

Within the test section, the wing's aerodynamic forces are measured through a six-degree-of-freedom Nano25 load cell, with an SI-250-6 calibration. The six degrees include measurements of the x , y , and z axes of forces and moments. As only the forces are required, the load cell is calibrated with pre-measured weights to test its



(a) Test Section Setup - Full Render



(b) Test Section Setup - Perspective Render

Figure 4.2: Test Section Setups Rendered in SOLIDWORKS

validity prior to aerodynamic testing. The serial number of the load cell, FT-14627, must be plugged into its respective data acquisition box, which also acts as a power source. For measurements to occur, the load cell must be placed between two triangular load cell plates, with one side on the mount and the other on the gearbox. To further validate the direction of the load cell and ensure the axes align correctly as expected, a slight force is induced in a particular axis and observed on the computer display. This helps confirm the orientation of the axes through a simple sanity check.

Motor and Controller

This leads to the last part of the setup, which is the motor that actuates the flapping of the wing, shown in **Figure 3.10**. Flapping is caused by the spinning of a 2280-kilovolt Brushless Direct Current (BLDC) motor, which directly spins the gears. The kilovolt rating describes that the motor spins 2280 rotations per minute per voltage supplied from a power supply unit. Regulated by an Electronic Speed Controller (ESC), the motor speed depends on the voltage passed through by the ESC. A flight computer, ‘SpearLily’ designed by Choudhury, has custom controls to change the throttling speed through Pulse Width Modulated (PWM) signals [41]. Further detail is mentioned in his thesis.

In its essence, the wing can be controlled remotely by three commands: angular increment, flapping frequency, and a stopping request. The angular increment, a scalar input value in degrees, spins the main gear in **Figure 3.10** by approximate input provided (dependent on battery voltage, as it drains and is not consistent with the output [41]). Furthermore, the flapping frequency is simply an input value for the number of oscillations per second (of the main gear) and is yet again dependent on battery voltage. Finally, the stopping request stops any ongoing commands no matter what condition, in the case any component breaks inside the wind tunnel.

4.2 Testing and Post Processing

This section details the testing procedures, including what is being tested and the method of post-processing and interpreting raw measured data.

4.2.1 Test Types

For the overall goals of this thesis, there are two main tests, pseudo-static and dynamic tests. Prior to these, there are a series of benchmarking tests to gather critical information on the model. This includes the gearbox drag at various wind speeds, membraneless runs for inertial force measurements (no wind), as well as dry runs with the membrane at different frequencies. The benchmarking test variables are summarised in **Table 4.1**. More specifically, these tables represent the independent variables changed to test the effects of the forces measured in the load cell. As the gearbox is a bluff body, it will inherently induce drag, depending on the velocity [55]. Therefore the induced drag on the gearbox is measured when by itself at a variety of wind tunnel speeds, as shown in **Table 4.1a**, and then subtracted from the raw measured values from the load cell. The dry run test variables, shown in **Table 4.1b**, describe the measurement of forces when the wing is fully assembled and flapping at different frequencies. Essentially, this helps confirm whether the measured values are expected or not without any aerodynamic forces. Lastly, the membraneless run in **Table 4.1c** measures the force of inertia at different frequencies, which should be subtracted to help purely visualise aerodynamic forces - an area no literature explores.

Table 4.1: Benchmarking Tests for Gearbox Drag, Dry Run, and Membraneless Run

(a) Gearbox Drag			(b) Dry Run Forces			(c) Membraneless Run		
Test	Value	Unit	Test	Value	Unit	Test	Value	Unit
8	m/s		1.0	Hz		1.0	Hz	
10	m/s		1.5	Hz		1.5	Hz	
12	m/s		2.0	Hz		2.0	Hz	
14	m/s		2.5	Hz		2.5	Hz	

Static and Dynamic Tests

As mentioned previously, two main tests are conducted: pseudo-static and dynamic tests.

detail both tests: how, what, why

define phase angle etc talk about the parameterization of each
include tables for each

make reference to the 3x3 figure of phase angles

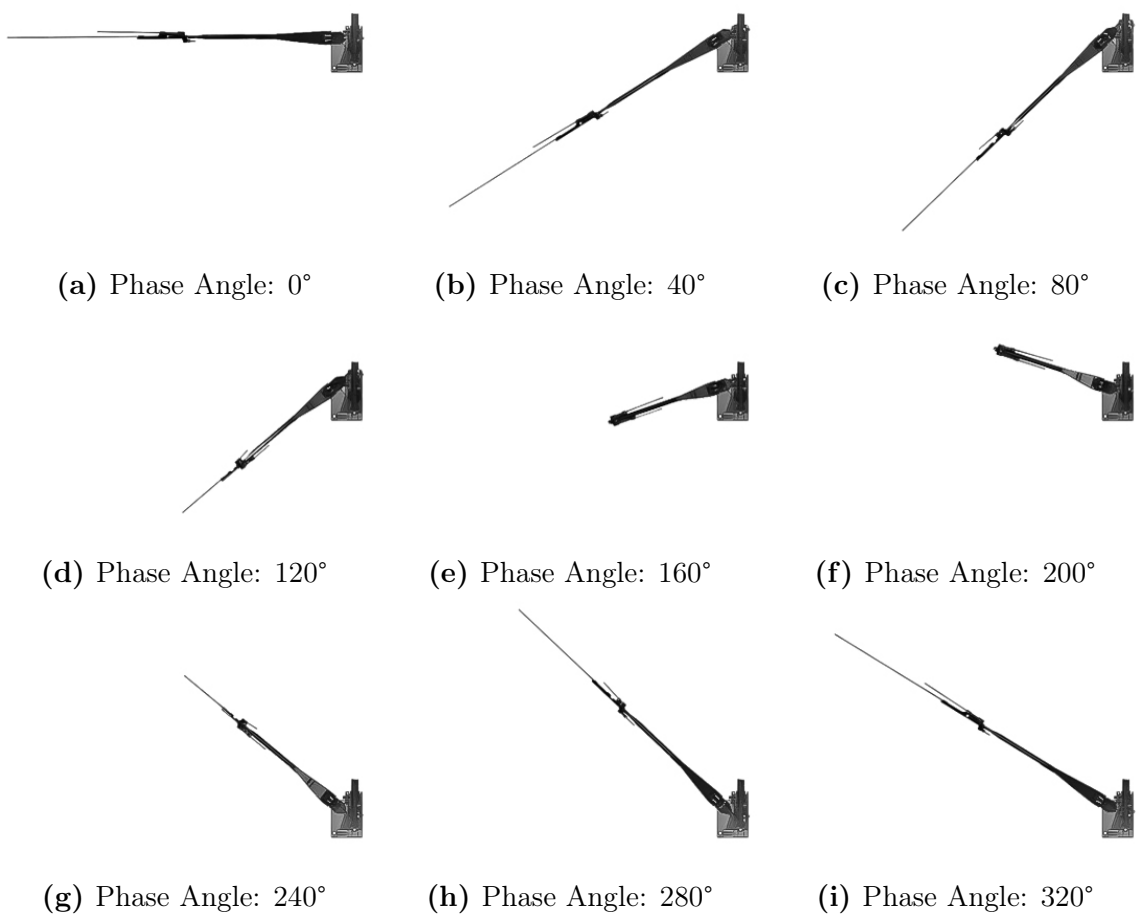


Figure 4.3: CAD Representation of Phase Angles

4.2.2 Post Processing

This page is intentionally left blank.

Chapter 5

Results and Discussion

5.1 Baseline Results

5.2 Pseudo-Static Results

5.3 Dynamic Results

5.4 Comparison with Analytical Results

This page is intentionally left blank.

Chapter 6

Conclusions

6.1 Final Thoughts

6.2 Further Improvements

6.3 Contributions and Achievements

Bibliography

- [1] C. D. Güss, S. Ahmed, and D. Dörner, “From da Vinci’s Flying Machines to a Theory of the Creative Process,” en, *Perspectives on Psychological Science*, vol. 16, no. 6, pp. 1184–1197, Nov. 2021, Publisher: SAGE Publications Inc, ISSN: 1745-6916. DOI: [10.1177/1745691620966790](https://doi.org/10.1177/1745691620966790). [Online]. Available: <https://doi.org/10.1177/1745691620966790>.
- [2] J. Anderson, *EBOOK: Fundamentals of Aerodynamics (SI units)*. McGraw hill, 2011.
- [3] K. M. Laurent, B. Fogg, T. Ginsburg, *et al.*, “Turbulence explains the accelerations of an eagle in natural flight,” *Proceedings of the National Academy of Sciences*, vol. 118, no. 23, e2102588118, 2021.
- [4] R. Dudley, *The biomechanics of insect flight: form, function, evolution*. Princeton university press, 2002.
- [5] J. M. Rayner, “Form and function in avian flight,” in *Current ornithology*, Springer, 1988, pp. 1–66.
- [6] C. J. Pennycuick, *Bird flight performance: a practical calculation manual*. Oxford University Press, 1989.
- [7] Z. Dyer, *Photo & Film / Zac Dyer / United Kingdom*, en. [Online]. Available: <https://www.zacdyer.com>.
- [8] sparrow, *Carolina wren in spring*. pl, Aug. 2016. [Online]. Available: <https://www.istockphoto.com/pl/zdj%C4%99cie/strzy%C5%BCyk-gm587939552-100957383>.
- [9] J. J. Videler, *Avian flight*. Oxford University Press, 2006.

- [10] *Figure 3. Typical wing tip paths during one wingbeat for a passerine... en.* [Online]. Available: https://www.researchgate.net/figure/Typical-wing-tip-paths-during-one-wingbeat-for-a-passrine-bird-and-a-small-bat-seen-in_fig2_24174968.
- [11] B. W. Tobalske, “Biomechanics of bird flight,” *Journal of Experimental Biology*, vol. 210, no. 18, pp. 3135–3146, 2007.
- [12] U. Norberg and J. Rayner, “Ecological morphology and flight in bats: Wing adaptations, flight performance, foraging strategy and echolocation. philosophical transactions of the royal society of london, b.,” *Biological Sciences*, vol. 316, pp. 335–427, 1987.
- [13] G. Spedding, “The aerodynamics of flight,” *Mechanics of animal locomotion*, vol. 11, pp. 52–111, 1992.
- [14] P. C. Withers, “An aerodynamic analysis of bird wings as fixed aerofoils,” *Journal of Experimental Biology*, vol. 90, no. 1, pp. 143–162, 1981.
- [15] D. A. Spera, “Models of Lift and Drag Coefficients of Stalled and Unstalled Airfoils in Wind Turbines and Wind Tunnels,” Tech. Rep. E-16599, Oct. 2008, NTRS Author Affiliations: Jacobs Technology Inc. NTRS Document ID: 20090001311 NTRS Research Center: Glenn Research Center (GRC). [Online]. Available: <https://ntrs.nasa.gov/citations/20090001311>.
- [16] M. Sadraey, “Drag Force and Drag Coefficient,” en,
- [17] J. B. Barlow, W. H. Rae, and A. Pope, *Low-Speed Wind Tunnel Testing*, en. John Wiley & Sons, Feb. 1999, Google-Books-ID: nUHWDwAAQBAJ, ISBN: 978-0-471-55774-6.
- [18] N. Rott, “Note on the History of the Reynolds Number,” en,
- [19] B. R. Munson, A. P. Rothmayer, and T. H. Okiishi, *Fundamentals of fluid mechanics*. Wiley Global Education, 2012.
- [20] H. Schlichting (Deceased) and K. Gersten, *Boundary-Layer Theory*, en. Springer, Oct. 2016, Google-Books-ID: bOUyDQAAQBAJ, ISBN: 978-3-662-52919-5.
- [21] L. Cattafesta, C. Bahr, and J. Mathew, “Fundamentals of Wind-Tunnel Design,” en, in *Encyclopedia of Aerospace Engineering*, R. Blockley and W. Shyy, Eds., 1st ed., Wiley, Dec. 2010, ISBN: 978-0-470-75440-5 978-0-470-68665-2. DOI: [10](https://doi.org/10.1002/9780470754405).

- 1002/9780470686652.eae532. [Online]. Available: <https://onlinelibrary.wiley.com/doi/10.1002/9780470686652.eae532>.
- [22] D. Auld, *Virtual Wind Tunnel Specifications*. [Online]. Available: https://www.aeromech.usyd.edu.au/snr/vt_specs.html.
- [23] R. D. Mehta and P. Bradshaw, “Design rules for small low speed wind tunnels,” en, *The Aeronautical Journal*, vol. 83, no. 827, pp. 443–453, Nov. 1979, ISSN: 0001-9240, 2059-6464. DOI: [10.1017/S0001924000031985](https://doi.org/10.1017/S0001924000031985). [Online]. Available: <https://www.cambridge.org/core/journals/aeronautical-journal/article/abs/design-rules-for-small-low-speed-wind-tunnels/600999B496885D7383AB1B04CFF9F4C0>.
- [24] B. Ma, G. Wang, Z. Ye, and L. Xu, “A numerical Method for Transonic Wind Tunnel Wall Interference Correction in Airfoil Testing,” in *34th AIAA Applied Aerodynamics Conference*, _eprint: <https://arc.aiaa.org/doi/pdf/10.2514/6.2016-3575>, American Institute of Aeronautics and Astronautics. DOI: [10.2514/6.2016-3575](https://doi.org/10.2514/6.2016-3575). [Online]. Available: <https://arc.aiaa.org/doi/abs/10.2514/6.2016-3575>.
- [25] W. R. Sears, “Self correcting wind tunnels,” en, *The Aeronautical Journal*, vol. 78, no. 758-759, pp. 80–89, Mar. 1974, ISSN: 0001-9240, 2059-6464. DOI: [10.1017/S0001924000036496](https://doi.org/10.1017/S0001924000036496). [Online]. Available: <https://www.cambridge.org/core/journals/aeronautical-journal/article/abs/self-correcting-wind-tunnels/EEA6698DE94276099F20FD2F19C6C26D>.
- [26] M. Houbreken, “The effect of formulation on the volatilisation of plant protection products,” Ph.D. dissertation, Jan. 2018.
- [27] E. F. Jaguaribe, “The Flat Plate Boundary Layer Equation under Blasius Restrictions with a Unique Solution,” en, *Mathematical Problems in Engineering*, vol. 2022, no. 1, p. 9032974, 2022, _eprint: <https://onlinelibrary.wiley.com/doi/10.1155/2022/9032974>, ISSN: 1563-5147. DOI: [10.1155/2022/9032974](https://doi.org/10.1155/2022/9032974). [Online]. Available: <https://onlinelibrary.wiley.com/doi/abs/10.1155/2022/9032974>.

- [28] B. F. R. Ewald, Ed., *Wind tunnel wall correction: = (La correction des effets de paroi en soufflerie)* (AGARDograph 336), en. Neuilly sur Seine: AGARD, 1998, ISBN: 978-92-836-1076-2.
- [29] I. Ross and A. Altman, “Wind tunnel blockage corrections: Review and application to Savonius vertical-axis wind turbines,” *Journal of Wind Engineering and Industrial Aerodynamics*, vol. 99, no. 5, pp. 523–538, May 2011, ISSN: 0167-6105. DOI: [10.1016/j.jweia.2011.02.002](https://doi.org/10.1016/j.jweia.2011.02.002). [Online]. Available: <https://www.sciencedirect.com/science/article/pii/S0167610511000377>.
- [30] A. Chen, B. Song, Z. Wang, D. Xue, and K. Liu, “A novel actuation strategy for an agile bioinspired fwav performing a morphing-coupled wingbeat pattern,” *IEEE Transactions on Robotics*, vol. 39, no. 1, pp. 452–469, 2022.
- [31] J.-S. Lee and J.-H. Han, “Experimental study on the flight dynamics of a bioinspired ornithopter: Free flight testing and wind tunnel testing,” *Smart Materials and Structures*, vol. 21, no. 9, p. 094 023, 2012.
- [32] M.-F. Scibilia and J. Wojciechowski, “Experimental study of aerodynamic behavior in wind tunnels with ornithopter and plane models,” *Journal of Thermal Science*, vol. 15, pp. 54–58, 2006.
- [33] T. N. Pornsirin-Sirirak, S. Lee, H. Nassef, *et al.*, “Mems wing technology for a battery-powered ornithopter,” in *Proceedings IEEE thirteenth annual international conference on micro electro mechanical systems (Cat. No. 00CH36308)*, IEEE, 2000, pp. 799–804.
- [34] S. Srigrarom and W.-L. Chan, “Ornithopter type flapping wings for autonomous micro air vehicles,” *Aerospace*, vol. 2, no. 2, pp. 235–278, 2015.
- [35] W. Send, M. Fischer, K. Jebens, R. Mugrauer, A. Nagarathinam, and F. Scharstein, “Artificial hinged-wing bird with active torsion and partially linear kinematics,” *28th Congress of the International Council of the Aeronautical Sciences 2012, ICAS 2012*, vol. 2, pp. 1148–1157, Jan. 2012.
- [36] A. Hedenström, L. Johansson, and G. Spedding, “Bird or bat: Comparing airframe design and flight performance,” *Bioinspiration & biomimetics*, vol. 4, p. 015 001, Apr. 2009. DOI: [10.1088/1748-3182/4/1/015001](https://doi.org/10.1088/1748-3182/4/1/015001).

- [37] E. Home, *Lectures on Comparative Anatomy; in which are Explained the Preparations in the Hunterian Collection*, en. Nicol, 1814, Google-Books-ID: jS-NCAAAcAAJ.
- [38] D. Lee, *Biomimicry: Inventions Inspired by Nature*, en. Kids Can Press Ltd, Aug. 2011, Google-Books-ID: Pnf2vUJjNCQC, ISBN: 978-1-55453-467-8.
- [39] L. H. Hyman, *Hyman's Comparative Vertebrate Anatomy*, en. University of Chicago Press, Sep. 1992, Google-Books-ID: VKIWjdOkiMwC, ISBN: 978-0-226-87013-7.
- [40] Salix, *Français : Face inférieure d'une aile. Chauve-souris de grenier, Charente-Maritime (France)English: Wing underside. Attic bat, Charente-Maritime (France)*, Oct. 2011. [Online]. Available: https://commons.wikimedia.org/wiki/File:Bat-wing_underside.jpg.
- [41] O. Choudhury, “Experimental validation of morphing ornithopter wings,” Nov. 2024.
- [42] K. Szwedziak, T. Łusiak, R. Bąbel, *et al.*, “Wind Tunnel Experiments on an Aircraft Model Fabricated Using a 3D Printing Technique,” en, *Journal of Manufacturing and Materials Processing*, vol. 6, no. 1, p. 12, Feb. 2022, Number: 1 Publisher: Multidisciplinary Digital Publishing Institute, ISSN: 2504-4494. DOI: [10.3390/jmmp6010012](https://doi.org/10.3390/jmmp6010012). [Online]. Available: <https://www.mdpi.com/2504-4494/6/1/12>.
- [43] S. Jia, Z. Zhang, H. Zhang, C. Song, and C. Yang, “Wind Tunnel Tests of 3D-Printed Variable Camber Morphing Wing,” en, *Aerospace*, vol. 9, no. 11, p. 699, Nov. 2022, Number: 11 Publisher: Multidisciplinary Digital Publishing Institute, ISSN: 2226-4310. DOI: [10.3390/aerospace9110699](https://doi.org/10.3390/aerospace9110699). [Online]. Available: <https://www.mdpi.com/2226-4310/9/11/699>.
- [44] R. Schütze, “Lightweight carbon fibre rods and truss structures,” *Materials & Design*, vol. 18, no. 4, pp. 231–238, Dec. 1997, ISSN: 0261-3069. DOI: [10.1016/S0261-3069\(97\)00056-3](https://doi.org/10.1016/S0261-3069(97)00056-3). [Online]. Available: <https://www.sciencedirect.com/science/article/pii/S0261306997000563>.
- [45] J. Zhang, G. Lin, U. Vaidya, and H. Wang, “Past, present and future perspective of global carbon fibre composite developments and applications,” *Compos-*

- ites Part B: Engineering*, vol. 250, p. 110463, Feb. 2023, ISSN: 1359-8368. DOI: [10.1016/j.compositesb.2022.110463](https://doi.org/10.1016/j.compositesb.2022.110463). [Online]. Available: <https://www.sciencedirect.com/science/article/pii/S1359836822008368>.
- [46] W. (H. Ward, “Design of a lightweight camping cot using carbon fiber tent poles and ripstop nylon,” eng, Accepted: 2007-03-12T17:44:22Z, Thesis, Massachusetts Institute of Technology, 2006. [Online]. Available: <https://dspace.mit.edu/handle/1721.1/36686>.
- [47] G. R. Behera, A. Mukhopadhyay, and M. Sikka, “Development of scheme to evaluate the performance of parachute canopy fabrics under tensile impact,” en, *Journal of Industrial Textiles*, vol. 51, no. 2_suppl, 2283S–3305S, Jun. 2022, Publisher: SAGE Publications Ltd STM, ISSN: 1528-0837. DOI: [10.1177/15280837221080103](https://doi.org/10.1177/15280837221080103). [Online]. Available: <https://doi.org/10.1177/15280837221080103>.
- [48] P. Paul and L. Paul, “An overview on the parachute recovery systems with additive manufacturing for UAV safe landing,” *Materials Today: Proceedings*, 2nd International Conference on Sustainable Materials, Manufacturing and Renewable Technologies 2022, vol. 72, pp. 3158–3162, Jan. 2023, ISSN: 2214-7853. DOI: [10.1016/j.matpr.2022.10.229](https://doi.org/10.1016/j.matpr.2022.10.229). [Online]. Available: <https://www.sciencedirect.com/science/article/pii/S2214785322067529>.
- [49] A. Săliștean and C. Mihai, “Textile wing fabric for emergency response UAS,” en, *Industria Textila*, vol. 71, no. 04, pp. 321–326, Aug. 2020, ISSN: 12225347. DOI: [10.35530/IT.071.04.1762](https://doi.org/10.35530/IT.071.04.1762). [Online]. Available: http://revistaindustriatextila.ro/images/2020/4/004%20ADRIAN%20SALISTEAN_Industria%20Textila%204_2020.pdf.
- [50] K. Mao, W. Li, C. J. Hooke, and D. Walton, “Friction and wear behaviour of acetal and nylon gears,” *Wear*, 17th International Conference on Wear of Materials, vol. 267, no. 1, pp. 639–645, Jun. 2009, ISSN: 0043-1648. DOI: [10.1016/j.wear.2008.10.005](https://doi.org/10.1016/j.wear.2008.10.005). [Online]. Available: <https://www.sciencedirect.com/science/article/pii/S0043164809001501>.
- [51] A. J. Muminovic, N. Pervan, M. Delic, E. Muratovic, E. Mesic, and S. Braut, “Failure analysis of nylon gears made by additive manufacturing,” *Engineering*

- Failure Analysis*, vol. 137, p. 106 272, Jul. 2022, ISSN: 1350-6307. DOI: [10.1016/j.engfailanal.2022.106272](https://doi.org/10.1016/j.engfailanal.2022.106272). [Online]. Available: <https://www.sciencedirect.com/science/article/pii/S1350630722002461>.
- [52] E. H. Tümer and H. Y. Erbil, “Extrusion-Based 3D Printing Applications of PLA Composites: A Review,” en, *Coatings*, vol. 11, no. 4, p. 390, Apr. 2021, Number: 4 Publisher: Multidisciplinary Digital Publishing Institute, ISSN: 2079-6412. DOI: [10.3390/coatings11040390](https://doi.org/10.3390/coatings11040390). [Online]. Available: <https://www.mdpi.com/2079-6412/11/4/390>.
- [53] B. van Magill, *CO₂ Laser Cutting / AMME Labs Wiki*. [Online]. Available: <https://wiki.ammelabs.org/fablab/technologies/cnc/co2lasercutting>.
- [54] B. Emmerson, “Post-Stall Performance of Cambered Airfoils,” en, 2024. [Online]. Available: <https://ses.library.usyd.edu.au/handle/2123/32263>.
- [55] A. ROSHKO, “On the Wake and Drag of Bluff Bodies,” *Journal of the Aeronautical Sciences*, vol. 22, no. 2, pp. 124–132, 1955, Publisher: American Institute of Aeronautics and Astronautics _eprint: <https://doi.org/10.2514/8.3286>. DOI: [10.2514/8.3286](https://doi.org/10.2514/8.3286). [Online]. Available: <https://doi.org/10.2514/8.3286>.

This page is intentionally left blank.

Appendices

A Progress to Date

A.1 Investigation into Tucking Kinematics

With the experimental objective being the development of a series of wing articulations in Wind Tunnel experimental tests, it is far more efficient to work on the development of an ornithopter wing that is able to control its extension variability. As such, with the development of the ornithopter wing articulation mechanism is designed, as depicted in **Figure A.1**, designed by Omrik and Adnan. The mechanism encompasses a large range of lateral motion, to mimic the articulation of bird wing extension and tucking.

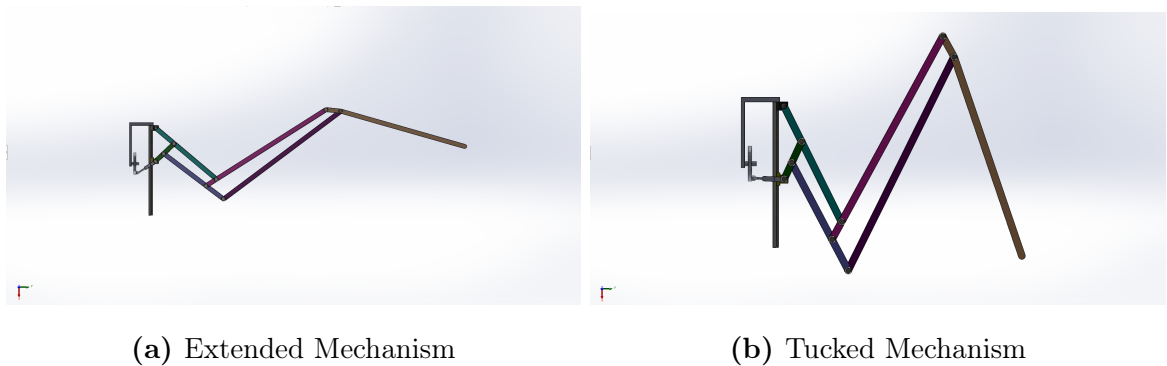


Figure A.1: CAD Prototype Ornithopter Mechanism

The mechanism incorporates two degrees of freedom, controlling both the flapping and tucking articulation with the control of the conical rocker mechanism designed by Chen et al. [30]. The models represented in **Figure A.1** showcase the transferred design to fit the requirements of this project. As such, with rotational control over the driving gear, the wing flap and tucking mechanism are dependent 90° out of phase. This best

represents the wing articulation found in avian flight.

The wing model is then translated to a 3D printed mechanism, seen in **Figure A.2**, to best outline key properties that may not have been understood when modelling. The structure was printed from PLA, using FDM printing for a highly iterative and flexible design and manufacture medium. Joints are fixed with M4 steel bolts, threading into the plastically deformed filament material. Early manufacturing products of the design show glaring overlap in mechanism joints, which may become problematic when incorporating additional spars. Additionally, the fixture of the joints using the steel bolts creates high friction within the joints. Although this may not be viable for the dynamic articulation of the wing, in steady-state regimes, the rigidity of the wing may actually work in the prototype's favour.



Figure A.2: 3D printed wing mechanism

Concerns regarding the current wing design have been highlighted when working on computational and material models. The proposed mechanism is light but structurally fragile which may be a point of failure for the project. There is a lot of proposed work that is yet to be incorporated into the wing spars, including fabric integration, fastener redesigns, and kinematic lineages for additional spars. As such, it is proposed that the next iteration of the wind design be fabricated via CNC machining with low-grade aluminium. The rationale behind this approach is to ensure structural integrity for an increasingly more complex design with time.

A.2 Progress Tracking

With regard to the progress as of now with the project, outlined in **Figure A.3** depicting the original Gantt chart, comments can be made on the adherence to the proposed timeline. All preliminary stages have been completed, from the literature review structure to the outline of potential designs. This is shown with the manufacturing of the preliminary model based on tucking articulation mechanisms and the coupling relationship to flapping motion.

Research is still required on the work towards a locking mechanism on the wing for testing against larger Reynolds numbers and on wing membrane integration into the model.

Hence, there is a discrepancy observed in the current progress of the proposal. Considering, the expectations of accelerated workflow during the outlined breaks, the proposed Gantt chart does not require adjustments. This is rationalised by lagging in only the wind tunnel plan and further preliminary design work.

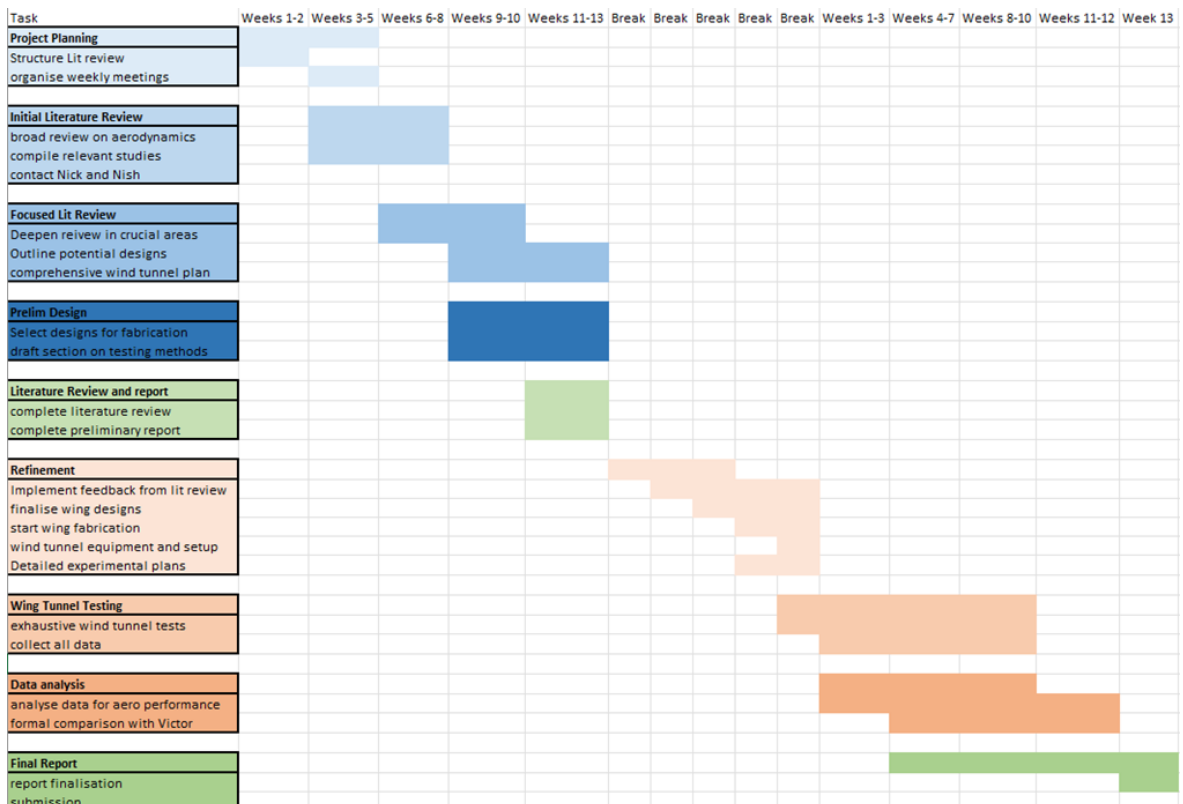


Figure A.3: Proposed Gantt Chart

A.3 Proceeding Semester work

Outlined in the Gantt chart is the proposed work for the next semester of university coursework regarding this project. The aim is to focus primarily on the manufacturing and refinement of the wing models that are the focus of wind tunnel testing.